PPPL--2426
DE87 013212

LOWER HYBRID EXPERIMENTS ON PLT USING GRILLS HAVING VARIOUS $n_{\parallel}$ SPECTRAL WIDTHS

By

J.E. Stevens, R. Bell, S. Bernabei, A. Cavallo, T.K. Chu, P. Colestock, W. Hooke, J. Hosea, F. Jobes, T. Luce, E. Mazzucato, R. Motley, R. Pinsker, S. von Goeler, and J.R. Wilson

MAY 1987

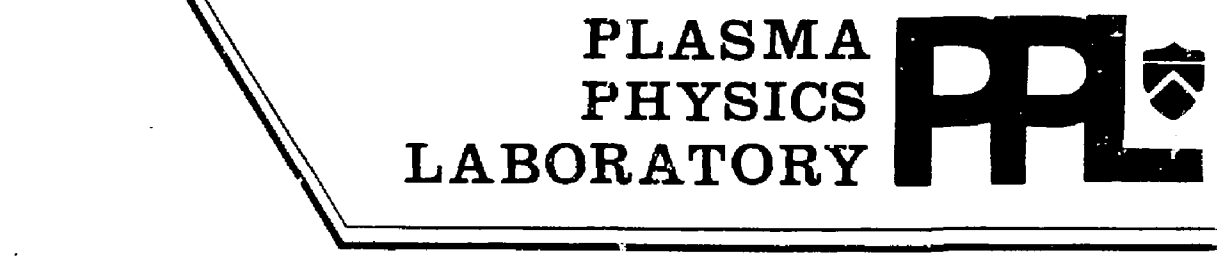

PRINCETON UNIVERSITY
PRINCETON, NEW JERSEY

PREPARED FOR THE U.S. DEPARTMENT OF ENERGY,
UNDER CONTRACT DE-AC02-76-CHO-3073.

NOTICE

Printed in the United States of America

Available from:

National Technical Information Service
U.S. Department of Commerce
5285 Port Royal Road
Springfield, Virginia 22161

Price Printed Copy $ * ; Microfiche $4.50

*Pages	NTIS Selling Price
1-25	$7.00
25-50	$8.50
51-75	$10.00
76-100	$11.50
101-125	$13.00
126-150	$14.50
151-175	$16.00
176-200	$17.50
201-225	$19.00
226-250	$20.50
251-275	$22.00
276-300	$23.50
301-325	$25.00
326-350	$26.50
351-375	$28.00
376-400	$29.50
401-425	$31.00
426-450	$32.50
451-475	$34.00
476-500	$35.50
500-525	$37.00
526-550	$38.50
551-575	$40.00
567-600	$41.50

For documents over 600 pages, add $1.50 for each additional 25-page increment.

LOWER HYBRID EXPERIMENTS ON PLT USING GRILLS HAVING VARIOUS $n_\parallel$ SPECTRAL WIDTHS

J.E. Stevens, R. Bell, S. Bernabei, A. Cavallo, T.K. Chu, P. Colestock, W. Hooke, J. Hosea, F. Jobes, T. Luce, E. Mazzucato, R. Motley, R. Pinsker, S. von Goeler, and J.R. Wilson

ABSTRACT

Coupling structures for lower hybrid current drive experiments have, until now, been smaller than a free space wavelength and have had a correspondingly broad wave number spectrum. In this paper we report the results of experiments on the PLT tokamak using a 16-waveguide grill (2.2 wavelengths) which produces a very narrow $n_\parallel = k_\parallel c/\omega$ spectrum. Experimental results from the 16-waveguide grill are compared with results from three other PLT grills with less sharply defined $n_\parallel$ spectra. The current drive figure of merit, $I_p \bar{n}_e R/P_{rf} \approx 0.14 \times 10^{14}$ A cm^{-3} m/W, is $\approx 40\%$ higher for the 16-waveguide coupler than for previously reported experiments on PLT, in spite of the larger "spectral gap."

1. INTRODUCTION

Lower hybrid experiments have made considerable progress in recent years towards the goal of experimentally achieving rf-driven currents in tokamak plasmas consistent with theoretical predictions.[1-5] In addition to maintaining steady-state currents without an ohmic transformer,[6-9] experiments have also demonstrated the ability of lower hybrid waves to start up[10-12] and ramp up[13-16] the tokamak plasma current as well as to heat electrons during current drive.[17-21] Experimental results are consistent with the predicted

velocity space behavior of the electron distribution function.[22-23] Plasma currents at the megampere level have now been driven by lower hybrid waves.[24] Steady-state current drive efficiencies are within a factor of two of theoretical predictions,[25] and a theory has been developed to explain rf current drive results in the presence of an electric field.[26-28] A comprehensive review of the current drive field has been given by Fisch.[29]

Since high power requirements[30] may make steady-state noninductive current drive impractical in large, reactor-grade tokamaks, one goal of recent experiments has been to maximize current drive efficiency. This was one of the purposes for constructing the 16-waveguide grill described in this paper. However, even if the goal of steady-state noninductive current drive proves impractical, rf current drive would still have many uses. First, a very modest lower hybrid system could replace the ohmic transformer in the low density current start-up and ramp-up phases of tokamak operation. Most of the steady-state plasma current might then be driven as a by-product of fusion power production if a means such as the boctstrap current[31-34] proves to be practical. Another application of lower hybrid current drive is the modification of the plasma current profile to improve MHD stability as has recently been demonstrated by the suppression of sawteeth.[35-38] Finally, at reactor densities where $T_e \approx T_i$, bulk electron heating as a by-product of current drive should be an effective heating method. Lower hybrid waves thus have a great potential in fusion research to initiate and drive currents and to heat electrons.

Coupling structures for lower hybrid current drive experiments have, until now, been smaller than a free space wavelength and have had a correspondingly broad $n_\parallel$ power spectrum. The launched $n_\parallel$ spectrum determines the main characteristics of lower hybrid wave experiments, including the

coupling, heating, and current drive efficiencies. In this paper we report the results of experiments on the PLT tokamak using a 16-waveguide grill which produces a very narrow $n_\parallel$ spectrum. Experimental results from the 16-waveguide grill are compared with results from three other PLT grills with less sharply defined $n_\parallel$ spectra. The current drive figure of merit, $I_p\bar{n}_eR/P_{rf} \approx 0.14 \times 10^{14}$ A cm^{-3} m/W, is $\approx$ 40% higher for the 16-waveguide coupler than for previously reported experiments on PLT, in spite of the larger "spectral gap"[6] and the reduced accessibility due to a higher frequency. In addition, handling and coupling were improved for the 16-waveguide coupler. The effect of the $n_\parallel$ spectrum on all aspects of current drive will be the main topic of this paper. Lower hybrid heating and sawtooth suppression experiments will be discussed elsewhere. The experiments with the 16-waveguide coupler, as well as unpublished results from previous experiments, will be discussed in the context of lower hybrid experiments on PLT from 1981-1986, using frequencies of 0.8 and 2.45 GHz, launched powers of up to 1 MW, and $n_\parallel$ spectral widths of 2.7, 1.55, 1.4, and 0.45. Experiments with the narrow $n_\parallel$ spectrum increase our understanding of how to improve the current drive and ramp-up efficiency, show the role of accessible versus inaccessible power, and emphasize the unimportance of the spectral gap.

The basic experimental setup is described in Sec. 2 of this paper. Results of coupling measurements are discussed in Sec. 3, current drive experiments in Sec. 4, ramp-up experiments in Sec. 5, and X-ray emission experiments in Sec. 6. A discussion and conclusion are given in Secs. 7 and 8.

2. THE EXPERIMENTAL SETUP

Lower hybrid experiments with four different couplers were carried out on the PLT tokamak between 1981 to 1986. The PLT tokamak operates with a major radius R = 1.32 m, a limiter minor radius of a = 0.40 m, a vacuum vessel minor radius of b = 0.50 m, a maximum toroidal field of 33 kG, and a plasma current of up to 770 kA.

The parameters of the four lower hybrid grills used on PLT are shown in Table I. The grill numbers listed in Table I, #1 through #4, will be used in parentheses throughout the text to identify the grill being discussed. For the 800-MHz grills (#1 & #2), each of six waveguides was fed by a Varian-VA955 klystron through 50 m of transmission line. The phasing was done at low power by variable phase shifters. The phases could also be changed during a pulse by switching the low level rf drive between varying lengths of cable. The 2.45-GHz grills (#3 & #4) were driven with three Varian VKS8269A klystrons located 50 m from the plasma. The phasing for the 2.45-GHz systems is accomplished by high power phase shifters located near PLT after the power is divided 8 ways.

From 1984 to 1985 the 2.45-GHz system (#3) consisted of two 8-guide grills located on top of the plasma and one grill located on the outside equatorial midplane. In 1986, the 16-guide grill (#4) was installed in an outside midplane port while keeping one of the 8-guide top grills. The 16-waveguide system (#4) was driven by two of the three klystrons. The phase could be varied arbitrarily in each of the 16 waveguides of the grill. The 16-waveguide, 2.45-GHz grill (#4) is shown in Fig. 1a from inside the vacuum vessel. The vacuum window for the 16-waveguide grill, shown in Fig. 1b, was the most satisfactory of the lower hybrid window designs used on PLT. It consisted of sixteen Al_2O_3 bricks brazed into a titanium-6242 alloy flange

with the same thermal expansion coefficient.[39] This window was reheated once to its 780°C braze temperature without damage to the ceramic bricks. The window was bolted directly to the stainless steel grill with rf waveguide continuity made by a simple butt contact to the 0.31-cm-thick grill walls. The window performed well from the mechanical, electrical, and vacuum perspectives.

The vacuum windows in all four grills were protected against arcing by a fault circuit which gated the rf power off for ~ 5-10 ms if the reflection coefficient in any waveguide exceeded a certain threshold (typically 60%-80%). New grills and windows were gradually brought to full power in 100-1000 rf pulses. After a new grill achieved full power, rf faults were generally not a problem for the typical power densities given in Table I unless unusual or rapidly changing plasma edge conditions were present.

3. WAVEGUIDE COUPLING

A major attraction of the lower hybrid wave for plasma heating was that a simple waveguide array[40] can transmit rf power efficiently into the plasma and that Brambilla's theory[41] accurately predicts the conditions for this efficient coupling to occur. The success of the theory in predicting the grill reflection allows us to infer that the actual spectrum is close to that predicted theoretically. This inference from coupling measurements is important because direct measurements of the wave position and wavelength inside tokamak plasmas, such as with CO_2 laser scattering,[42] are rare. Usually only indirect indications of the $n_\parallel$ spectrum inside the plasma are available. These indirect measurements, such as the slope of the hard X-ray tail,[7] comparing top and side launching,[43] and comparing current drive efficiency versus waveguide phasing all are consistent with a launched $n_\parallel$

spectrum close to that predicted by Brambilla. This spectrum, modified by ray tracing, determines the major characteristics of lower hybrid experiments. Only the filling of the spectral gap between the velocity of the bulk electrons and the waves is not explained by coupling theory and first-pass ray tracing. However, the existence of the spectral gap has little effect on the experimental results.

Brambilla's theory predicts the fraction of reflected power in each guide as well as the shape of the launched $n_{\parallel}$ spectrum, given an edge density or density gradient in front of the coupler. As a general rule, the most efficient coupling occurs for an edge density given by

$$n_{EDGE} \sim n_c \, n_{\parallel o}^2 \quad , \tag{1}$$

where $n_c \equiv \omega^2 m_e / 4\pi e^2$ is the critical density for the wave frequency ω and $n_{\parallel o}$ is the peak of the launched $n_{\parallel}$ spectrum determined approximately by the waveguide phase difference, $\Delta\phi$, free space wavelength λ_o, and the waveguide spacing W:

$$n_{\parallel o} \simeq \frac{\lambda_o}{W} \frac{\Delta\phi}{360^\circ} \quad . \tag{2}$$

A secondary peak at $n_{\parallel} \simeq \lambda_o/W(\Delta\phi - 360^\circ)/360^\circ$ contains power going in the opposite toroidal direction. This secondary peak usually contains a small amount (~ 10%) of the total power for $\Delta\phi \sim 90^\circ$, while at $\Delta\phi = 180^\circ$ it contains the same power as the primary peak. The peak of the launched power spectrum is characterized by a width at half maximum of

$$\Delta n_{\parallel} = \frac{\lambda_o}{L} \quad , \tag{3}$$

where $L = N \times W$ is the total width of the array of N guides.

Figure 2 is a plot of the launched $n_{\parallel}$ spectra calculated for each of the PLT couplers in Table I. The phasings plotted were optimum for current drive. Spectra for other phasings have similar half-widths with their peak $n_{\parallel}$'s shifted according to Eq. (2). Shifts in the $n_{\parallel}$ spectrum due to toroidal ray propagation should not be a factor for most of the experiments discussed in this paper. A small ($\approx$ 10%) upshift in the launched $n_{\parallel}$ spectrum occurs from plasma edge to plasma center for waves launched from the outside midplane. However, the $n_{\parallel}$ spectrum for waves making multiple passes through the plasma could be greatly altered.

Measurements of reflection for each waveguide were monitored for all of the grills used on PLT (Table I). The waveguide grills were located in the scrape-off plasma 3-5 cm outside the limiter radius, and were generally excited with a fixed phase difference $\Delta\phi$ between adjacent guides. The most detailed comparison with theory was carried out with the 800-MHz-wide grill (#1 in Table I). Coupling measurements on the later grills (#2-#4) were carried out only to the extent necessary to ensure that the grill phasing was properly calibrated.

Figure 3a shows reflection versus phase for three different positions of grill #1 along with theoretical curves[44] assuming plasma edge densities which give the best fit to the data. These assumed densities are in approximate agreement with edge densities measured by probes. Figure 3b shows the measured reflection versus the distance from the grill to the plasma center. Both the grill position and the plasma position were varied, with the plasma position being varied by the vertical field. Since points with different

grill positions and different plasma positions overlay on one curve, this result indicates that moving the plasma has almost the same effect on coupling as moving the grill. The experimental data show the expected minimum of reflection versus grill position (or versus edge density). The theory curve, assuming a 2.5-cm-density scrape-off length, shows qualitatively the same behavior as the experimental data. Figure 3c shows reflection for the two inside guides (3 and 4) and the two outside guides (2 and 5) for the same shots as plotted in Fig. 3b. The measured reflections are again qualitatively similar to theoretical calculations (solid lines), which show the reflection minimum for the outside guides occurring at a lower density than for the inside guides.

For the 800-MHz "narrow" grill (#2 in Table I) and for both of the 2.45-GHz grills (#3 and #4), a shorted $\lambda_o/8$ waveguide was added on each side of the array. These passive guides behave like a low-power-driven guide with a 90° phase delay from the adjacent driven guide. The passive guides reduce the reflected power in the last active guide of the array, as demonstrated by earlier experiments.[45] The shorted $\lambda/8$ waveguides also protect the grill from damage due to plasma bombardment.

Measurements of reflection versus phasing for grills #2 and #3 also agree well with Brambilla's theory. A reflection versus phase curve at $\approx$ 1 kW/cm^2 for one 2.45-GHz, 8-guide grill (#3) is shown in Fig. 3d. Systematic coupling versus phase scans were no longer carried out for the 16-waveguide grill (#4). However, data for one scan at $\approx$ 3 kW/cm^2, in which the plasma conditions did not vary with phase, are plotted in Fig. 8d along with a theoretical curve for the 16-guide grill. Also, experience at many different individual plasma and phase conditions indicates that the phase calibrations are correct. For instance, at a plasma density of 1 x 10^{13}cm^{-3}, low

reflections ($R < 10\%$) could be achieved in all 16 waveguides for all phase differences in the range $60° < \Delta\phi < 300°$. Without a plasma load $R > 90\%$ was observed for $\Delta\phi = 75°$. When $\Delta\phi$ was set to 60°, so that part of the spectrum begins to overlap $n_{\parallel} = 1$, then the reflection coefficient in all 16 waveguides increased to $\approx 20\%$ and high power operation became difficult. Phases with $\Delta\phi < 60°$ could not be used in the presence of a plasma because the high reflections caused the arc sense circuits to switch the rf off. Finally, if one group of 8 guides had a phase difference discontinuity from the second group of 8, then the reflection in waveguides 8 and 9 was high as predicted by theory.

Typical operating power densities as well as typical reflection coefficients for those power densities are indicated in Table I. These "typical" power densities could be achieved on most days after a few (< 10) plasma shots. At these typical power levels, it was found that the average reflection decreases as the spectrum width $\Delta n_{\parallel}$ decreases (Table I). Coupling calculations show that it is possible to find model edge densities with small reflections for each of the four couplers, but in practice this was true only at low power (< 20 kW/guide). As power was increased to >40 kW/guide, the 16-waveguide grill maintained a lower reflection coefficient than the other grills listed in Table I.

The peak power densities indicated in Table I could be achieved during relatively constant plasma discharges after half a day's running (~ 75 shots). Precautions that were taken during high power operation included coating the waveguides with a thin layer of carbon to help suppress secondary multipactor emission,[46] locating the grill well away from the plasma limiters and gas feed valve, and rounding the surfaces of the grill which faced the plasma.

The stainless steel surfaces inside the 16-waveguide grill (#4) were copper plated, since multipactor breakdown is less of a problem for the dimensions of that grill and since copper has higher conductivity than stainless steel and also adsorbs less H_2 and D_2 gas. The 16-waveguide grill operated at nearly full power after one day of running, and was not subject to window arcing. The 16-waveguide grill was able to operate at a single radial position for line average plasma densities between 2×10^{12} and 5×10^{13} cm^{-3}, although the overall reflection coefficient increased to ~ 20% near both extremes. This increased reflection could presumably have been compensated for by moving the grill position, although no attempt was made to do so. At $\bar{n}_e \sim 1 \times 10^{13}$ cm^{-3}, overall reflection for the 16-guide grill was typically 5% for 700 kW of net power (~ 3 kW/cm^2). The coupling for the 16-waveguide grill was by far the best of the four grills used on PLT.

4. STEADY-STATE CURRENT DRIVE

Fisch[1] has shown theoretically that lower hybrid current drive is characterized by a figure of merit η_{CD} given by

$$\frac{I_p n_e R}{P_{rf}} \sim \eta_{CD}(n_\parallel, T_e, Z_{eff}) \frac{A \cdot 10^{14}\ cm^{-3} \cdot m}{W} \quad , \tag{4}$$

where I_p is the plasma current, n_e the electron density, R the tokamak major radius, P_{rf} the rf power, and η_{CD} is a function, whose value is of order 1, of the $n_\parallel$ spectrum, T_e, the bulk electron temperature, and Z_{eff}, the average ion charge state. Figure 4, adapted from Karney and Fisch,[26] shows the function η_{CD} for several values of T_e and Z_{eff} plotted versus $n_\parallel$. The value η_{CD} in Fig. 4 is obtained by a relativistic Fokker-Planck calculation assuming that

the $n_\parallel$ spectrum is narrow. We will now proceed to show how the experimental results compare with these theoretical predictions.

The characteristics of steady-state current drive were studied for all of the couplers used on PLT (#1-#4). A typical steady-state current drive discharge using the 16-waveguide grill is shown in Fig. 5. Figure 5a shows a 520-kA discharge that is initiated and maintained with the ohmic (OH) transformer until 0.4 seconds, after which the OH primary current is maintained constant. A net rf power of 520 kW from the 16-waveguide grill holds the current constant from 0.4-0.7 seconds. The grill is phased with $\Delta\phi = 75°$, which produces the spectrum shown in Fig. 2. All of the other discharge characteristics were held nearly constant during the rf pulse to ensure an accurate measurement of the current drive figure of merit. Figure 5b shows a constant density of 1×10^{13} cm^{-3} during the rf pulse. Figure 5c shows power input to the plasma from inductive sources (solid line) and from the rf. The inductive power dissipated in the plasma is the power induced from the external ohmic and vertical field transformers minus the change in plasma magnetic energy:

$$P_{IND} = \left(M_{OH}\frac{dI_{OH}}{dt} + M_{SF}\frac{dI_{SF}}{dt}\right)I_p - \frac{d}{dt}\left(\frac{1}{2}LI_p^2\right) \quad , \tag{5}$$

where

$$L = \mu_o R\left(\ell n\frac{8R}{a} - 2 + \ell_i/2\right) \tag{6}$$

and $\ell_i/2$ is derived from the plasma equilibrium position signal $\Lambda = \beta_p + \ell_i/2$ shown in Fig. 5d. In Eqs. (5)-(6), M_{OH} and M_{SF} are the mutual inductances

between the OH and vertical field coils and the plasma, I_{OH} and I_{SF} are the OH and vertical field primary currents, L is the plasma inductance, R is the major radius, and a is the minor radius. Since $\beta_p = 1/2(\beta_\parallel + \beta_\perp)$ is not measured directly, it is estimated from kinetic measurements of the plasma energy content, with major contributions from both the plasma bulk and the high energy electron tail. Bulk electron energy content is measured with Thomson scattering, bulk ion energy content is measured from neutron emission, and tail electron energy content is estimated from hard X-ray measurements for similar discharges.[22-23] For the curve of P_{IND} in Fig. 5c, $\beta_p \approx 0.2$ during the rf pulse and $\beta_p \approx 0.08$ for the other times. These values are consistent with the jump in Λ seen in Fig. 5d just after rf turn on (0.4-0.45 sec). The jump in Λ at rf turn on is attributed primarily to changing β_p, while the much slower changes in Λ are due to changing ℓ_i. The calculation of P_{IND} is not accurate during those times where β_p is changing rapidly (0.4-0.5 sec). Sharp features in the P_{IND} curve with time scales of less than 35 ms are not meaningful because of numerical averaging.

All measurements of the current drive figure of merit, η_{CD}, were made with P_{IND} as close to zero as possible to avoid electric field effects. A correction is made for small values of $P_{IND} \neq 0$ by simply adding P_{IND} to P_{rf}. Correcting for P_{IND} in this way probably underestimates η_{CD} when $P_{IND} < 0$ and overestimates η_{CD} when $P_{IND} > 0$, because the incremental conversion efficiency of rf into poloidal field energy is less than 100%. The current drive figure of merit for the discharge shown in Fig. 5 is calculated to be: $\eta_{CD} = I\bar{n}_{14}R/P_{rf} \approx 1.4$ during the time 0.5-0.7 seconds. A ~25 kW correction is made to P_{rf} in this case because $P_{IND} \approx -25$ kW during that time. The line average density, rather than simply density, is used in the definition of η_{CD} for the experimental results ($n_{eo} \approx 1.5\ \bar{n}_e$).

Several sources of error in the measurement of η_{CD} are present. The error in calculating P_{IND} should be < 5% of P_{rf} when all of the time-varying terms in Eq. (5) are near zero. Another source of error is a systematic ± 5% error in the measurements of P_{rf}.

Measurements of η_{CD} were made for all four PLT grills and the range of results are shown in Fig. 6, plotted versus density. The $n_{\parallel}$ spectra, shown in Fig. 2, were optimized for best current drive for each set of data from the four grills. The vertical width of the bands represents the day-to-day irreproducibility of the data. We believe this to be caused by changes in the vacuum vessel surface conditions and plasma positioning. The current drive performance on PLT gradually improved with time after a vacuum opening. Several trends are apparent from Fig. 6:

Current drive versus spectral width - The best current drive figure of merit for each grill depends inversely on the spectral width of the grill. The 16-waveguide grill (#4) with by far the narrowest spectrum ($\Delta n_{\parallel} \sim 0.45$) is clearly the most effective for current drive, while the narrow 800-MHz grill (#2) with the widest spectrum ($\Delta n_{\parallel} \sim 2.7$) is the least effective for current drive. The 800-MHz-wide grill (#1) and the 2.45-GHz 8-waveguide grills (#3) have approximately the same spectral widths and approximately the same optimized current drive figure of merit.

Density limit for current drive - A very sharp drop in η_{CD} occurred with the 800-MHz system above the density of 7×10^{12} cm^{-3}. Parametric decay instability and a surface, fast ion tail occurred above that density, and the interaction of the rf with the electron tail decreased sharply as seen by the strongly decreasing emission at $2\,\Omega_{ce}$ and X-rays above 7×10^{12} cm^{-3}. The 2.45 system produced completely rf-driven currents at densities up to 1.5×10^{13} cm^{-3} and produced enhanced plasma X-ray and 2nd harmonic cyclotron

emission up to densities of 4.5×10^{13} cm^{-3}, at which density a fast ion tail again appeared. These results for 800 MHz and 2.45 GHz are consistent with the density limit for electron interaction observed on other machines,[47-48] i.e., the wave interacts with electrons when $f/f_{LH} \gtrsim 2$. Current drive figure of merit, η_{CD}, is plotted versus plasma density, current, temperature, and waveguide phasing in Fig. 7a-d for selected steady-state shots using the 16-waveguide grill in order to investigate these dependencies in more detail.

Current drive versus density and magnetic field (accessibility) - Although current drive theory (Eq. 4) predicts $\eta_{CD} \propto n_e$, Figs. 6 and 7a show a gradual drop in η_{CD} for increasing $\bar{n}_e$. The reason for this is that wave accessibility determines the minimum $n_\parallel$ at which wave interaction with electrons can take place for a given density and magnetic field. The accessible $n_\parallel$ for lower hybrid waves is given by[49]

$$n_{\parallel a} \approx 1 + f_{pe}^2/f_{ce}^2 - f_{pi}^2/f^2 + f_{pe}/f_{ce} \quad . \tag{7}$$

Evaluating $n_{\parallel a}$ at a minor radius $r/a \approx 1/2$, so that $\bar{n}_e \approx n_e(r/a = 1/2)$, results in $n_{\parallel a}$'s of 1.25-1.57 for $\bar{n}_e = 5 \times 10^{12}$-$2 \times 10^{13}$ cm^{-3} at B = 31 kG. The accessible $n_\parallel$ implies a maximum electron interaction energy given by $\varepsilon = (n_{\parallel a}/\sqrt{n_{\parallel a}^2 - 1})$, where ε = total electron energy normalized to mc^2. If we estimate the figure of merit as being determined approximately by slowing down of electrons at the maximum accessible energy, then we expect $\eta_{CD} \propto 1/n_\parallel^2 \equiv (\varepsilon^2 - 1)/\varepsilon^2$. This dependency is plotted in Fig. 7a for two magnetic fields (B = 31 kG and 21 kG). The proportionality constant for η_{CD} in the 31 kG curve is scaled to fit data from a density scan with I_p = 500 kA using the 16-guide grill (2/3 of P_{rf}) plus an 8-guide grill (1/3 of P_{rf}). The trend of the data fits the expectation of current drive efficiency limited by accessi-

bility. The 21-kG curve is plotted with the same proportionality constant along with a 21-kG data point for otherwise the same grill and plasma conditions, and it also scales with the expectations derived from wave accessibility.

The current drive figure of merit for the 800-MHz grill #1 was also consistent with wave accessibility.[50] However, the best values of η_{CD} for the 16-waveguide grill were systematically ≈ 40% higher than for the other PLT grills (#1-#3). This is in spite of the fact that the 800-MHz system (#1-#2) had slightly better accessibility than the 2.45-GHz system due to the larger f_{pi}^2/f^2 term in Eq. (7) for 800 MHz. This higher η_{CD} indicates that the 16-waveguide grill delivers its power more efficiently to the fastest electrons in the tail.

Current drive versus plasma current

Figure 7b is a plot of figure of merit η_{CD} versus steady-state current for the 16-waveguide grill at two different densities. At 1 x 10^{13} cm^{-3}, there is a decrease in η_{CD} at the lowest current (220 kA) but no significant difference between η_{CD} for the 520 kA and 770 kA cases. However, at 5 x 10^{12} cm^{-3}, η_{CD} for the 240 kA point is slightly higher than for the higher current (500 kA) case. Several important plasma parameters change when the plasma current is changed, i.e., plasma safety factor q_a, plasma temperature, and possibly Z_{eff}. Changes in these parameters may be responsible for the variation (or lack of variation) in η_{CD} with I_p. For example, the shots at the highest current level for both densities (770 kA at 1 x 10^{13} cm^{-3} and 500 kA at 5 x 10^{12} cm^{-3}) had a noticeable density rise during the rf pulse due to energetic electrons hitting the limiter. In addition, the 770 kA shot had impurities injected into the plasma during the rf pulse for spectroscopic studies. The resulting increase in Z_{eff}, inferred from plasma hard X rays,

could decrease η_{CD} for both cases. A rise in Z_{eff} of 1 theoretically makes an $\geq$ 10% change in figure of merit η_{CD} for our parameters. The plasma safety factor could also affect η_{CD} by changing the confinement properties of both the bulk and tail electrons. For the range of data in Fig. 7b, q_a varied from 2.5 to 8.

Current drive versus electron temperature - Variations in the current drive figure of merit of ≈ 10% might be expected from theory (Fig. 4) over the range of electron temperatures present in PLT (2 keV < T_e < 6 keV) during current drive. Current drive figure of merit η_{CD} is plotted versus peak electron temperatures in Fig. 7d for the same shots shown in Fig. 7b. For the data at $\bar{n}_e = 1 \times 10^{13}$ cm^{-3} in Fig. 7d (solid points), there is a 40% improvement in η_{CD} with temperature (2.3 vs. 4-5.3 keV). At the same time, plasma current is increasing from 220 kA to 520-770 kA. However, at 5×10^{12} cm^{-3}, the figure of merit is 12% smaller for the higher temperature (3.3 keV, 500 kA) shot than for the low temperature (2.3 keV, 220 kA) shot. For the same reasons as discussed above in connection with Fig. 7b, it is difficult to conclude that the variations in figure of merit are a result of temperature and not related to changes in other parameters.

In general, it was found that the fastest waves which were accessible on the first pass were optimum for current drive. A scan of η_{CD} versus phase is plotted in Fig. 7c for the 16-waveguide grill, with the 8-waveguide grill supplying one third of the rf power. The figure of merit, η_{CD}, was highest for $\Delta\phi$=75° ($n_{\parallel 0}$ = 1.5) and fell by ≈ 20% for $\Delta\phi$ =60° ($n_{\parallel 0}$ = 1.2) and $\Delta\phi$ = 90° ($n_{\parallel 0}$ = 1.8). The 20% reduction in efficiency at $\Delta\phi$ = 90° is consistent with the relative drop in phase velocity since $\eta_{CD} \propto 1/n_{\parallel}^2$. The $\Delta\phi$ = 60° case is complicated by having ≈ 50% of the launched spectrum inaccessible. The accessible part of the spectrum is consistent with a ≈ 33% drop in η_{CD} from

$\Delta\phi \approx 75°$, while the actual drop was $\approx 20\%$. This discrepancy could be due to some of the inaccessible power eventually finding its way into the plasma.

A comparison of the experimental current drive results with the theoretical curves of Fisch and Karney plotted in Fig. 4 requires several additional assumptions about the data. The parameters of the discharge shown in Fig. 5 are chosen to illustrate the comparison of the measured current drive efficiency η_{CD} with theory: $I_p = 520$ kA, $T_{eo} \approx 5$ keV, $\bar{n}_e = 1 \times 10^{13}$ cm^{-3}, $B_o = 31$ kG, $\eta_{CD} = 0.14$, and $n_\parallel = 1.5 \pm 0.45$. The extent of the accessible $n_\parallel$-spectrum is plotted as the double arrow in Fig. 4, labeled PLT. Three assumptions are made in plotting this line. First, the low $n_\parallel$ part of the spectrum is determined by wave accessibility to the plasma center. For $r/a \approx 1/2$, $n_{\parallel a} \approx 1.38$. Second, the high $n_\parallel$ side of the spectrum must extend to a high enough $n_\parallel$ to produce enough current carriers, i.e., $v_{ph} \approx 3\, v_{te}$. For $T_{eo} \lesssim 5$ keV, this occurs for $n_\parallel \gtrsim 2.5$. Finally, the experimental η_{CD} value of the PLT data is multiplied by 1.5 to account for an approximately parabolic density profile, since Fig. 4 plots density while the experimental measurements use line average density. The peak density is chosen since hard X-ray measurements indicate that most of the fast tail is located in the center of the plasma column.

The theoretical expectation for the PLT experiment is in the neighborhood of the point labeled A in Fig. 4. This point falls on the 5 keV, $Z = 4$ theoretical curve approximately in the center of the PLT spectrum. A value of $Z_{eff} \approx 3$-4 is typical of Thomson scattering measurements of Z_{eff} at $\bar{n}_e \approx 1 \times 10^{13}$cm^{-3} for ohmic plasmas. Also, previous hard X-ray measurements[23] are consistent with $Z_{eff} \approx 4$ for lower density, lower current rf-driven discharges. With the above assumptions, the experimental results are a factor of 0.67 ± 0.25 of the idealized theoretical calculation. However, other

inefficiency factors discussed below can account for the remaining 33% of the rf power.

One known inefficiency occurs because the grill launches only ≈ 90% of the rf power in the forward direction (P_F) and 10% of the rf power in the reverse direction (P_R). This backward spectrum drives an opposing current I_B, although at reduced (≈ 1/3) efficiency relative to the forward current (I_F). Thus, current drive efficiency scales as

$$\left(\frac{I}{P}\right)_{meas} \approx \frac{I_F - I_B}{P_F + P_B} \approx \frac{I_F - (0.11)\ 1/3\ I_F}{P_F + 0.11\ P_F} \approx 0.87\left(I_F/P_F\right)_{theory} .$$

This amount of backward current is consistent with a comparison of previous X-ray measurements with Fokker-Planck calculations which assumed only a forward spectrum (Fig. 9, Ref. 23). In that calculation there were not enough backward electrons to account for the observed backward X-ray emission. However, adding a backward tail with the relative amplitude given above (I_B/I_F ≈ 0.05) would bring the calculation into agreement with the X-ray measurements.

Another inefficiency is due to direct loss of tail electrons. Since the slowing-down time for fast electrons is comparable to the electron confinement time, some fraction of tail energy should be lost directly to the limiters. We have estimated ≈ 5% of the rf power is required to create an observed localized incandescent spot on the limiters, although we have no estimate of possible additional, more diffuse, losses.

Another power loss channel is cyclotron radiation. Calculations for a model electron distribution show that ≈ 5% of the rf power is radiated as cyclotron emission for our parameters. Finally, we cannot rule out the possibility that some power does not penetrate the plasma surface, although we do not have an estimate for this.

In summary, $\gtrsim$ 90% of the theoretically expected rf-driven current can be accounted for. However, there are many large sources of error for these measurements and calculations. Errors in Z_{eff} of ± 1, for instance, can make ± 10% differences in the results.

5. RAMP-UP EXPERIMENTS WITH THE 16-WAVEGUIDE GRILL

A short series of shots (~ 30) using the 16-waveguide grill was devoted to current ramp-up. This did not allow time for machine conditioning which might have allowed us to operate at the low densities ($\bar{n}_e \sim 2 \times 10^{12}$ cm^{-3}) of our previous experiments.[14-15] However, the same ramp-up efficiencies (≈ 20%) were obtained at densities of $\bar{n}_e \approx 3\text{-}5 \times 10^{12}$ cm^{-3}. Ramp-up efficiency is defined in the same way as previously[15]: $\text{eff} = -P_{IND}/P_{rf}$ where P_{IND} is given by Eq. (5) and is evaluated beginning 100 ms after rf turn on to avoid transients in $\Lambda = \beta_p + \ell_i/2$ due to changing β_p.

Figure 8a shows a ramp-up shot for $\bar{n}_e \approx 4.4 \times 10^{12}$ cm^{-3}, P_{rf} = 670 kW, I_p ≈ 200 kA, and $\dot{I}_p \approx 200$ kA/s. A large density rise occurs beginning 120 ms after rf turn on, due to fast electrons escaping the plasma and creating a localized hot spot on the limiter. This density rise occurred in PLT as the power levels and densities approached those of Fig. 8a. The large jump in $\beta_p + \ell_i/2$ occurring in Fig. 8a during the rf pulse is due primarily to the $\beta_\parallel$ of the fast electron tail. Data for a series of ramp-up shots at $\bar{n}_e = 5 \pm 0.5 \times 10^{12}$cm^{-3} and $I_p = 260 \pm 20$ kA are plotted in Figs. 8b-8d versus rf power. Ramp-up efficiency (Fig. 8b) was evaluated after the jump in $\beta_p + \ell_i/2$ until the density rise occurred. The rf pulse widths were limited by the density rise to 350 ms for $P_{rf} \leq 400$ kW and to 250 ms for the higher powers. The data for P_{rf} = 670 kW are uncertain because the period of time between the rf turn on and density rise is so short. The P_{IND} signal is most accurate

when averaged over longer ($\gtrsim$ 100 ms) times. Ramp-up efficiencies of $\approx$ 20% are observed when $P_{rf}/P_{steady\ state} \gtrsim 3$. This result is identical to previous experiments.[15] However, previous best ramp-up efficiencies with the 800-MHz system (grill #1) dropped sharply with density from 20% at 2×10^{12} cm^{-3}, to almost zero at 4×10^{12} cm^{-3}. With the 16-waveguide coupler, ramp-up efficiencies of 20% are observed from 3-5 $\times 10^{12}$ cm^{-3} and efficiencies of 10% were observed at 1×10^{13} cm^{-3}.

Peak and volume average electron temperatures are plotted in Fig. 8c, with averages taken over shots with similar rf power levels. The peak temperature increases from an ohmic value of 1.5 keV to a saturated level between 3-3.5 keV for $P_{rf} > 270$ kW. Average T_e increases slowly with P_{rf}. The calculated suprathermal current driven by the lower hybrid waves is plotted in Fig. 8d along with the integrated central hard X rays with energies $E > 35$ keV. The suprathermal current I_{st} is calculated by $I_{st} = I_p - I_B$ where I_B is the ohmic bulk (backward) current determined by $I_B = V_{axis}/R_\Omega$. The plasma resistance R_Ω is calculated from 26-point Thomson scattering (TVTS) profiles of electron temperature assuming that $Z_{eff} \approx 3$-4 measured during the ohmic phase is constant during the rf pulse. A $Z_{eff} = 4$ was chosen for the plot in Fig. 8d. The TVTS and hard X-ray measurements are taken before the density rise occurs. Hard X rays are measured along a vertical chord viewing through the plasma center, perpendicular to $\underline{B}_0$. The approximate linear increase of calculated I_{st} with P_{rf} is consistent with the increase in the hard X rays. Thus, at the highest power levels there are two large counterstreaming currents, $I_{st} \approx 500$ kA and $I_B = -230$ kA, which produce a slowly increasing plasma current $I_p = 270$ kA.

During steady-state current drive shots on PLT, X-ray and electron cyclotron emission signals reach a plateau $\sim$ 50 ms after rf turn on,

indicating that the tail reaches a steady state. However, during ramp-up, both of these signals continue to increase with time throughout the 250-350 ms rf pulses. The rate of increase of the ECE signal increased with rf power. This continuous increase may be indicative of a slow buildup of backward runaway electrons, which could possibly reduce the ramp-up efficiencies in Fig. 8b over longer ramp-up times (> 200 ms). Unfortunately, because these low density, high power ramp-up shots had a sharp density rise 100-300 ms after the beginning of the rf pulse, it cannot be determined how important this continuous buildup of the tail is to long time ramp-up efficiency.

The Fisch-Karney theory[25] was successful in interpreting previous PLT data in terms of a universal curve of P_{el}/P_{rf} versus v_{ph}/v_R, where $P_{el} = -P_{IND} + V^2_{axis}/R_\Omega$, P_{IND} is given by Eq. (5), $V_{axis} = P_{IND}/I_p$ is the loop voltage on axis, R_Ω is the (Spitzer) resistivity of the bulk plasma, $v_{ph} = c/n_\parallel$ is the average wave phase velocity, and v_R is the runaway velocity (Dreicer velocity without the Z dependence). Figure 9 shows how the recent ramp-up data with the 16-waveguide grill (#4) compare with the previous [28,52] data using grill #1 plotted on the Fisch-Karney diagram. The efficiency of the 16-waveguide, narrow spectrum grill is significantly higher than that of the previous data taken with a wider spectrum grill #1. The only adjustments to the data in this plot was to add a 10% upshift in peak $n_\parallel$, which is predicted by ray tracing to occur as the wave penetrates on the first pass (this shifts all the data points to 10% smaller v_{ph}/v_R). The theory curves assume 43% and 64% of the rf power is absorbed by the tail in order to fit the old and new data. Assuming that the theory is correct, there are two ways to interpret these results. One interpretation is that wave absorption is 50% better for the 16-waveguide grill, perhaps due to better wave penetration to the plasma center. The alternative interpretation is that the absorption is

the same for both grills, but that the average v_{ph} for wave-particle interaction is ~ 1.45 times higher for the 16-waveguide grill. The previous data from grill #1 would fall on the theory curve for 64% absorption if an additional $n_{\parallel}$ upshift factor of ~ 1.45 is assumed for those data. It is interesting to note that with this interpretation the ramp-up data imply a higher increase in efficiency for the 16-waveguide grill than that implied by the steady-state data. A 1.45 times lower $n_{\parallel}$ would imply a $(1.45)^2 = 2.1$ times increase in steady-state figure of merit for the 16-waveguide grill whereas only a factor of 1.4 increase was observed. Better absorption of the narrow spectrum during ramp-up may be a result of requiring more power for quasilinear flattening of the distribution function slope at high energies when a strong opposing electric field is present in addition to collisions.

In spite of the larger P_{el}/P_{rf} for a given v_{ph}/v_R achieved during ramp-up with the 16-waveguide grill (#4) relative to the previous 800-MHz grill (#1), the conversion of rf power into poloidal field energy remained at ≈ 20%, with the remaining power going into V^2/R_Ω dissipation of the back current.

The bulk plasma resistivity was measured with Thomson scattering profiles for the 16-waveguide grill (#4) ramp-up data, whereas R_Ω was only estimated for the 800-MHz ramp-up data using grill #1. Shots with $P_{rf} \approx 270$ kW were compared to check whether the V^2/R_Ω term in Fig. 9 was treated consistently for the two data sets. An estimated $R_\Omega \approx 2$ μΩ was used for the previous data compared with $R_\Omega \approx 2.5$ μΩ for the recent data. Since electron temperatures have tended to be higher for the 16-waveguide grill compared with previous grills, this implies that R_Ω may be slightly underestimated and V^2/R_Ω slightly overestimated for the previous 800-MHz data plotted in Fig. 9. Thus, the difference in P_{el}/P_{rf} between grills #1 and #4 is, if anything, understated by Fig. 9.

6. CURRENT PROFILES AND WAVE DAMPING

The X-ray emission profiles of the current-carrying tail give a good indication of the RF-driven component of the plasma current profiles in completely rf-driven tokamak discharges.[6] The primary factor affecting X-ray profile shape is the q_a of the plasma, with low q_a discharges having the broadest profiles. Figure 10 is a plot of integrated hard X-ray emission profiles ($E > 35$ keV) measured with a vertical 7-chord array for several limiter q_a values. These profiles are normalized to the same peak value so that the various profile shapes become apparent. The profiles with cylindrical $q_a = 8.2$, 3.6, and 2.5 were achieved with the 16-waveguide grill at $B = 31$-33 kG, $\bar{n}_e = 1 \times 10^{13}$ cm^{-3}, by varying I_p from 230 to 770 kA and P_{rf} from 260 to 680 kW. The X-ray radius at half maximum increases by 5 cm as q_a decreases from 8.2 to 2.5. Most of the wave spectrum was accessible for those three shots. The $q_a = 2.4$ X-ray profile was achieved with the 16-waveguide grill plus an 8-waveguide grill at $B = 21$ kG, $\bar{n}_e = 0.9 \times 10^{13}$ cm^{-3}, $I_p = 500$ kA, and $P_{rf} = 870$ kW. Approximately 50% of the launched power was inaccessible inside $r/a = 1/2$ for the 21 kG case. This may account for the wider profile. Radio-frequency power by itself had only a small effect on the X-ray profile. For example, the radius (at half maximum) of the X-ray profile broadened only by ~ 1 cm in the ramp-up scan of Fig. 8, as rf power increased from 130 to 680 kW. Plasma density also had a relatively small effect on the X-ray profile width. The radius at half maximum broadened by ≈ 1.5 cm as density increased from 6×10^{12} cm^{-3} to 1.55×10^{13} cm^{-3} for the scan shown in Fig. 7a.

It should be noted that the energy transport time τ_s from electron tail to bulk plasma is comparable to the bulk electron energy confinement time $\tau_E \sim \tau_s \sim 30$ msec for $n_e = 1.5 \times 10^{13}$ cm^{-3} on PLT.

7. DISCUSSION

The fact that the narrow $n_{\parallel}$ spectrum 16-waveguide grill improves wave coupling ($R \approx 5\%$) at typical operating power levels (~ 3 kW/cm^2) means that arrays with a large number of elements appear to be desirable. Low reflections are favorable for advanced grill designs such as the multijunction grill concept.[51] The multijunction grill greatly simplifies large, fixed $n_{\parallel}$ systems by replacing power dividers with simple H-plane partitions across the incident waveguide. Because reflected power in the individual waveguides of the multijunction configuration can cross couple to neighboring guides, large reflections from the plasma cannot be tolerated.

The fact that the current drive figure of merit depends so strongly on the launched spectrum supports the notion that much of the wave power is absorbed on the first pass through the plasma, at least during the steady-state phase of current drive. Multiple passes tend to upshift and randomize the launched $n_{\parallel}$ spectrum, so there should not be such a large difference between grills and grill phasings if first pass damping did not absorb much of the wave power. Calculations by Bonoli[54] predict strong ($\sim 50\%$), but not completed damping of low $n_{\parallel}$ components of the spectrum for grill #1. Current drive with the narrow $n_{\parallel}$ spectrum 16-waveguide grill (#4) was $\sim 40\%$ better than with the wider $n_{\parallel}$ grill (#1) indicating that first pass absorption of this fast, narrow spectrum is still quite strong. Since accessibility appears to limit the maximum wave phase velocity no matter what grill is used, then the 16-waveguide grill must improve the current drive figure of merit by either making the tail flatter and/or by optimizing the first pass delivery of the rf power spectrum to the plasma center.

The ramp-up results with the 16-guide grill are also consistent with both of these interpretations. The ramp-up data show that an ~ 1.45 factor

increase in $n_\parallel$ is required in order to fit the previous PLT data[28,52] onto the same Fisch-Karney efficiency curve as now fits the 16-waveguide grill data. This is in spite of the fact that the two sets of data have exactly the same peak $n_\parallel$. If the theory is assumed to be correct, then we can interpret the experimental result as an indication that either the narrow $n_\parallel$ spectrum produces a more energetic (flatter) tail or that the narrow $n_\parallel$ spectrum is absorbed better. Direct measurements of the tail distribution function, made by perpendicular viewing of both polarizations of electron cyclotron emission,[53] show that the 16-waveguide grill produces more tail electrons at energies greater than 90 keV ($n_\parallel < 1.9$) than the 8-waveguide grill.

The density rise problem encountered during low density, high power, and high current discharges appears to be due to the small scrape-off length of the escaping fast electrons and could probably be solved with a larger limiter surface area in contact with the plasma. Tokamaks such as PLT and Alcator-C, in which the plasma is bounded by a material limiter, appear to have more difficulty controlling the escaping fast electron tail than tokamaks with diverters such as ASDEX and JT-60.

The spectral gap question becomes more of an issue for the 16-waveguide grill than it was in previous experiments. In fact, the spectral gap was widest for the most efficient current drive shot, where $\eta_{CD} = 0.145$, $T_{e0} = 2.3$ keV, and $n_\parallel \approx 1.5 \pm 0.45$. Calculations show that < 3% of rf power was launched in the range $2 < n_\parallel < 3.5$ or alternatively $20\ keV < \varepsilon < 70\ keV$ for that shot. Model distribution functions which are flat over this range, which contain the minimum number of tail electrons required for stability, are calculated to dissipate at least ~ 10-15% of the rf power by collisions in the spectral gap. Mechanisms for filling this spectral gap have been proposed, such as (1) multiple wave passes through the plasma,[54] (2) the anomalous

Doppler instability driving plasma waves unstable,[55] (3) scattering and upshifting of the wave spectrum by edge density fluctuations,[56] and (4) by relying on the small amount of high $n_\parallel$ power launched by the grill.[57,58] In choosing among these explanations, we emphasize two, perhaps conflicting, experimental points: (1) the mechanism which fills the spectral gap works automatically, even over a very wide range of energies, while (2) narrowing the launched $n_\parallel$ spectrum has significantly improved the current drive effectiveness, which suggests that the launched spectrum is not being significantly dispersed by any of these gap filling mechanisms on the first pass through the plasma. These results probably favor the Bonoli mechanism,[54] because that mechanism allows strong first pass absorption while the spectral gap is filled in a self-regulating manner by the remaining $n_\parallel$-upshifted power.

Current drive with the widest $n_\parallel$ spectrum (grill #2, 800 MHz) had the poorest efficiency. How much of this is due to a nonoptimal spectral shape, i.e., too much power in the high $n_\parallel$ spectrum, or due to poor penetration because of strong Landau damping is difficult to determine. Estimates of the damping length of the high $n_\parallel$ component of the launched wave spectrum are difficult because the slope of the forward plateau of the tail distribution function has not been measured accurately enough. The range of slopes consistent with X-ray measurements, from $T_\parallel \sim 500$ keV to exactly flat, imply radial Landau damping lengths from ~ 1 cm to infinity. Experiments done on ASDEX using a two-peaked spectrum have demonstrated that the high $n_\parallel$ part of the spectrum adds very little to the current drive produced by the low $n_\parallel$ part of the spectrum,[59] while experiments with two grills on Petula suggest that filling the spectral gap with a high $n_\parallel$ launched spectrum does improve overall current drive efficiency.[60]

Operating in cleaner ($Z_{eff} \rightarrow 1$), hotter ($T_e \sim 10$ keV) plasmas could theoretically increase η_{CD} by a factor of ~2-3 over that achieved in PLT. The point labeled "B" in Fig. 4 is such an operating condition. A further factor of two in η_{CD} could be achieved at even higher T_e (~ 25 keV) or lower $n_\parallel$ (≈ 1). However, the difficulty at higher T_e is that quasilinear wave damping becomes very strong for $v_{ph} \lesssim 2.5\ v_{te}$, while lower hybrid wave accessibility will prevent $n_\parallel$ from approaching 1.

Finally, significant improvements in peak electron temperatures ($T_{eo} \approx 6$ keV) have been achieved during electron heating experiments at 2.45 GHz with the 16-waveguide grill over what was achieved with the wider-$n_\parallel$ grill #3 (≈ 4 keV).[21] This again suggests better wave penetration into the plasma with the narrow $n_\parallel$ grill.

Further narrowing of the launched spectrum to $\Delta n_\parallel \sim 0.1$ should be achievable in larger machines with higher frequency systems. However, the grill may have to be tilted at an angle of approximately $a/q_a R \sim 1/10$ so that the grill remains parallel to the field lines over its entire width.

8. CONCLUSION

The narrow spectrum of the PLT 16-waveguide grill leads to significantly improved lower hybrid coupling, current drive figure of merit, electron heating, and ramp-up efficiency P_{el}/P_{rf} at a given v_{ph}/v_R. The practical ramp-up efficiency of converting rf power into poloidal field energy remained at ~ 20% for the 16-waveguide grill. Additional gains (factors of ~ 2-4) in current drive figure of merit depend (theoretically) more on having the wave $n_\parallel$ approach 1 in a clean ($Z = 1$), hot ($T_e > 10$ keV) plasma than on further reductions in spectral width. However, further reductions in spectral width may be desirable for lower hybrid waves to achieve better quasilinear penetration in hot plasmas as well as to achieve better coupling.

ACKNOWLEDGMENTS

The authors would like to express our appreciation to the PLT technical support staff, the high power rf engineering staff, and the data acquisition staff for their hard work in support of this experiment. We thank J. Boychuk, E. Evans, K. Mann, J. Siegel, and R. Sorenson for their efforts in constructing the lower hybrid system. We thank H.P. Furth, P.H. Rutherford, D. Meade, and K. Bol for their support of this work. This work was supported by U.S. Department of Energy Contract No. DE-AC02-76-CHO3073.

REFERENCES

[1]N. Fisch, Phys. Rev. Lett. 41 (1978) 873.

[2]T. Yamamoto, T. Imai, M. Shomada, N. Suzuki, M. Maeno, et al., Phys. Rev. Lett. 45 (1980) 716.

[3]M. Nakamura, T. Cho, S. Kubo, T. Shimozuma, H. Kawai, et al., Phys. Rev. Lett. 47 (1981) 1902.

[4]T. Maekawa, T. Saito, M. Nakamura, T. Cho, S. Kubo, et al., Phys. Lett. 85A (1981) 339.

[5]S. Luckhardt, M. Porkolab, S. Knowlton, K.I. Chen, A.S. Fischer, et al., Phys. Rev. Lett. 48 (1982) 152.

[6]S. Bernabei, C. Daughney, P. Efthimion, W. Hooke, J. Hosea, et al., Phys. Rev. Lett. 49 (1982) 1255.

[7]W. Hooke, S. Bernabei, D. Boyd, A. Cavallo, T.K. Chu, et al., in Plasma Physics and Controlled Nuclear Fusion Research 1982, Vol. I, p. 239 (IAEA-CN-41/C-5).

[8]M. Porkolab, J.J. Schuss, Y. Takase, S. Texter, B. Blackwell et al., Op. Cit. p.227.

[9]M. Porkolab, J.J. Schuss, B. Lloyd, Y. Takase, S. Textor, et al., Phys. Rev. Lett. 53 (1984) 450.

[10]S. Kubo, M. Nakamura, T. Cho, S. Nakao, T. Shimozuma, et al., Phys. Rev. Lett. 50 (1983) 1994.

[11]F. Jobes, J. Stevens, R. Bell, S. Bernabei, A. Cavallo, et al., Phys. Rev. Lett. 52 (1984) 1005.

[12]K. Toi, K. Ohkuba, K. Kawahata, Y. Kawasumi, K. Matsuoka, et al., Phys. Rev. Lett. 52 (1984) 2144.

[13]J. Stevens, S. Bernabei, M. Bitter, F. Boody, et al., Proc. of the 3rd Joint Varenna-Grenoble Int. Symp. on Heating in Toroidal Plasmas, (Pergamon Press, New York, 1982) Vol. II (1982) p. 455.

[14]R. Motley, R. Bell, S. Bernabei, A. Cavallo, T.K. Chu, et al., in Plasma Physics and Controlled Nuclear Fusion Research, 1984 (IAEA, London, 1984) Vol. I., p. 473.

[15]F. Jobes, S. Bernabei, T.K. Chu, W. Hooke, E. Meservey, et al., Phys. Rev. Lett. 55 (1985) 1295.

[16]F. Leuterer, D. Eckhartt, F. Söldner, G. Becker, K. Bernhardi, et al., Phys. Rev. Lett. 55 (1985) 75.

[17]M. Porkolab, B. Lloyd, Y. Takase, P. Bonoli, C. Fiore et al., Phys. Rev. Lett. 53 (1984) 1229.

[18]D. van Houtte, G. Agarici, P. Blanc, P. Briand, G. Briffod, et al., Proc. 4th Conference on Heating in Toroidal Plasmas, Roma, I (1984) 554.

[19]F. Alladio, M. Apicella, E. Barbato, G. Bardotti, R. Bartiromo, et al., Proc. of the 9th International Conference on Plasma Physics and Controlled Nuclear Fusion Research, Baltimore, MD (1982), IAEA 12, 41.

[20]F. Söldner, D. Eckhardt, F. Leuterer, K. McCormick, G. Becker et al., Proc. 13th European Conference on Controlled Fusion and Plasma Physics, Schliersee, 1986.

[21]S. Bernabei, R. Bell, A. Cavallo, T.K. Chu, P. Colestock, et al., in Proc. of the 11th International Conference on Plasma and Controlled Nuclear Fusion Research, (1986).

[22]S. von Goeler, J. Stevens, S. Bernabei, M. Bitter, T.K. Chu, et al., Nucl. Fusion 25 (1985) 1515.

[23]J. Stevens, S. von Goeler, S. Bernabei, M. Bitter, T.K. Chu, et al., Nucl. Fusion 25 (1985) 1529.

[24]JT-60 TEAM, Proc. of the 11th International Conference on Plasma and Controlled Nuclear Fusion Research, Kyoto, Japan (1986), IAEA-CN-47-/K-I-2.

[25]C.F.F. Karney and N.J. Fisch, Phys. Fluids 22 (1979) 1817.

[26]C.F.F. Karney and N.J. Fisch, Phys. Fluids 29 (1986) 180; also N.J. Fisch, Phys. Fluids 29 (1986) 172.

[27]N.J. Fisch and C.F.F. Karney, Phys. Rev. Lett. 54 (1985) 897.

[28]C.F.F. Karney, N.J. Fisch, and F.C. Jobes, Phys. Rev. A. 32 (1985) 2554.

[29]N.J. Fisch, Rev. Modern Phys. 59 (1987) 175.

[30]D.A. Ehst, Nucl. Fusion 25 (1985) 629.

[31]R.J. Bickerton, J.W. Conner, and J.B. Taylor, Nature 229 (1971) 110.

[32]A.A. Galeev and R.Z. Sagdeev, Plasma Phys. and Controlled Nuclear Fusion 1, 481 (Conf. Proceedings, Madison, 1971) IAEA, Vienna, 1971; Nucl. Fusion supplement (1972) 45.

[33]B.B. Kadomtsev and V.D. Shafranov, Plasma Phys. and Controlled Nuclear Fusion Research 2, 479 (Conf. Proceedings, Madison, 1971) IAEA, Vienna, 1971; Nucl. Fusion supplement (1972) 209.

[34]Ya.I. Kolesnichenko, S.N. Reznik, and V.A. Yavorskij, Nucl. Fusion 20 (1980) 1041.

[35]T.K. Chu, R. Bell, S. Bernabei, A. Cavallo, W. Hooke, in Sixth Topical Conf. on RF Plasma Heating, Pine Mountain, GA (1985).

[36]C. Gormezano, P. Blanc, H. Bottollier, P. Briand, G. Briffod, et al., in Sixth Topical Conference on RF Plasma Heating, Pine Mountain, GA (1985).

[37]K. McCormick, B. Bartiromo, H.S. Bosch, M. Brambilla, H. Derfler, et al., in Controlled Fusion and Plasma Physics (Proc. 12th European Conference, Budapest, 1985) Vol. I (1985) 199.

[38]F. Söldner, D. Eckhardt, F. Leuterer, K. McCormick, G. Becker, et al., in Proceedings of 13th European Conference on Controlled Fusion and Plasma Physics, Schliersee, April 1986.

[39]R. Walls and E. Evans, "High Temperature Brazing of Al_2O_3 to Ti6242," private communciation.

[40]P. Lallia, Proc. of 2nd Topical Conf. on RF Plasma Heating, Paper C-3, Lubbock, TX (1974).

[41]M. Brambilla, Nucl. Fusion 16 (1976) 47.

[42]R.L. Watterson, Y. Takase, P. Bonoli, M. Porkolab, R. Slusher, and C. Surko, Phys. Fluids 28 (1985) 2622.

[43]S. Bernabei, R. Bell, T.K. Chu, A. Cavallo, et al., Nucl. Fusion 26 (1986) 111.

[44]J. Stevens, M. Ono, R. Horton, J.R. Wilson, Nucl. Fusion 21 (1981) 1259.

[45]R. Motley S. Bernabei, W. Hooke, F. Paoloni, Nucl. Fusion 20 (1980) 1207.

[46]J. Timberlake, S.A. Cohen, C. Crider, G. Estepp, W. Hooke, et al., J. Vac. Sci. Technol. 20 (1982) 1309.

[47]M. Mayberry, M. Porkolab, K.I. Chen, A.S. Fischer, D. Griffin, et al., Phys. Rev. Lett. 55 (1985) 829.

[48]F. Alladio, F. Crisanti, G. Bardotti, R. Bartiromo, G. Bracco, et al., in 11th European Conf. on Controlled Fusion and Plasma Physics, Aachen, Sept. 1983.

[49]V.E. Golant, Sov. Phys., Tech. Phys. 16 (1972) 1980.

[50]R. Motley, S. Bernabei, T.K. Chu, W. Hooke, D. Ignat, et al., Proc. of 6th Topical Conf. on RF Plasma Heating, Madison WI (1982).

[51]C. Gormezano, P. Briand, G. Briffod, G.T. Hoang, T.K. N'Guyen, D. Moreau, G. Ray, Nucl. Fusion 25 (1985) 419.

[52]F.C. Jobes, S. Bernabei, T.K. Chu, N.J. Fisch, W.M. Hooke et al., in Tokamak Startup, ed. H. Knoepfel, Ettore Majorana, International Science Series, Physical Sciences 26 203 (1985).

[53]T. Luce and P. Efthimion, Bull. Am. Phys. Soc. 31 (1986) 1468.

[54]P.T. Bonoli and R.C. Englade, Phys. Fluids 29 (1986) 2937.

[55]C. Liu, V.S. Chan, D.K. Bhadra, and R.W. Harvey, Phys. Rev. Lett. 48 (1982) 1479.

[56]P.L. Andrews and F.W. Perkins, Phys. Fluids 26 (1983) 2537.

[57]S. Succi, K. Appert, J. Vaclavik, and D. Moreau, in 10th Intern. Conf. on Plasma Physics and Controlled Nuclear Fusion Research, London, UK (September 1984).

[58]V.K. Decyk, Third European Workshop on Problems in the Numerical Modelling of Plasmas, Varenna, Italy (September 1985).

[59]F. Leuterer, M. Brambilla, D. Eckhartt, K. McCormick, M. Munich, F. Söldner et al., in Proceedings of 13th European Conference on Controlled Fusion and Plasma Physics Schliersee, April 1986.

[60]F. Parlange, G. Agarici, P. Blanc, H. Bottollier-Curtet, P. Briand et al., in Proceedings of 12th European Conference on Controlled Fusion and Plasma Physics, Budapest, Vol. II (1985) p. 172.

Table I Lower Hybrid Couplers on PLT

Grill (or coupler)	#1	#2	#3	#4
Dates	1981-84	1983	1984-86	1986
Frequency	0.8 GHz	0.8 GHz	2.45 GHz	2.45 GHz
N-guides	6	6	8	16
Grill Position	side	side	2 top, 1 side	side
Guide Height	22 cm	22 cm	10 cm	11 cm
Guide Width	3.5 + 0.6 cm	2.0 + 0.3 cm	1.0 + 0.1 cm	1.4 + 0.3 cm
$n_{\parallel o}$ (90°)	2.25	4.1	2.7	1.8
$\Delta n_{\parallel}$ (F.W.H.M.)	1.55	2.7	1.4	0.45
$P_{typical}$	0.75 kW/cm^2	1 kW/cm^2	3 kW/cm^2	3 kW/cm^2
P_{max}	2.1 kW/cm^2	2 kW/cm^2	4.5 kW/cm^2	3 kW/cm^2 (max. available)
Guide Coating	stainless steel and carbon	carbon	stainless steel and carbon	Copper
Window from Plasma	54 cm	54 cm	20 cm	40 cm
$R_{typical}$	15-25%	20-30%	10-15%	3-7%
Grill Minor Radius (limiter = 40 cm)	44-45 cm	44-45 cm	42-43 cm	43 cm

Figure Captions

Fig. 1(a) The 16-waveguide grill viewed from inside the PLT torus. (b) The vacuum window for the 16-waveguide grill. Each ceramic window is 1.4 cm × 11 cm.

Fig. 2 Spectra for the four grills used on PLT from 1981-86. The phasings ($\Delta\phi$) shown were optimum for current drive.

Fig. 3 Coupling characteristics for the PLT grills. (a) Total reflection versus phase difference for the 800-MHz-wide grill (#1). Densities assumed for the theory curves give best fit to the data. (b) Total reflection versus coupler to plasma center distance for grill #1 with $\Delta\phi$ = 180°. The theory curve, assuming a 2.5-cm-density scrape-off length, shows qualitatively the same behavior. (c) Reflection for inside and outside waveguides. (d) Reflection versus phase difference for the 2.45-GHz, 8-waveguide grill (#3) at 90 kW forward power and 16-guide (#4) at 680 kW forward power. The plasma was moved towards the coupler for the 16-guide, $\Delta\phi$ = 180° point.

Fig. 4 Theoretical current drive figure of merit assuming $\Delta n_{\parallel} \to 0$ and Z_{eff} = 1 and Z_{eff} = 4 (dashed) (from Karney and Fisch). The curve parameters are bulk electron temperature in keV. The arrow represents the extent of the launched spectrum of the PLT 16-waveguide grill (#4). "A" represents the best result which can be expected in PLT if all of the experimental inefficiencies could be eliminated and "B" represents the optimum for a 10 keV, Z_{eff} = 1 reactor.

Fig. 5 Current drive shot showing (a) plasma current, (b) line average density, (c) power dissipation in plasma, (d) $\Lambda = \beta_p + \ell_i/2$, and (e) loop voltage versus time. The ohmic heating primary current is held fixed from 0.4 to 0.9 sec., and the rf power drives the plasma current from 0.4 to 0.7 sec.

Fig. 6 Range of data for the current drive figure of merit versus density for the four grills used on PLT.

Fig. 7 (a) Current drive figure of merit (η_{CD}) versus line average density at B = 31 kG (solid points) and B = 21 kG (triangle). The curves are calculated assuming η_{CD} is determined by slowing down of electrons at the maximum accessible energy. The rf power came from the 16-guide grill (2/3 P_{rf}, $\Delta\phi$ = 75°) and from an 8-guide grill (1/3 P_{rf}, $\Delta\phi$ = 60°). (b) Figure of merit versus plasma current for the 16-waveguide grill ($\Delta\phi$ = 75°) at two densities. (c) Figure of merit versus phasing of the 16-waveguide grill, with the 8-waveguide grill supplying 1/3 of the rf power at $\Delta\phi$ = 60°. The theory curve is derived by integrating $n_\parallel^{-2}$ over the first pass accessible spectrum of both grills. (d) Figure of merit versus bulk electron temperature for the same shots as in Fig. 7b.

Fig. 8 (a) Ramp-up shot using 16-waveguide coupler. (b) Ramp-up efficiency versus rf power. (c) Peak electron temperature versus power for shots in Fig. 8b. (d) Central hard X ray ($\varepsilon > 60$ keV) emission versus power for shots in Fig. 8b-c.

Fig. 9 Plot of P_{el}/P_{rf} versus v_{ph}/v_R for data taken with the 16-waveguide grill (#4) (solid dots) and the 800-MHz grill #1 (crosses). The only adjustment to the data is a 10% upshift in peak $n_{\parallel}$ assumed when calculating v_{ph}. Theory curves assume 43% (solid) and 64% (dashed) absorption of the launched rf power. The fraction of P_{el} converted into poloidal field energy is indicated approximately by the dotted line.

Fig. 10 Hard X-ray profiles for completely rf-driven discharges with cylindrical q_a = 8.2, 3.6, 2.5, and 2.4.

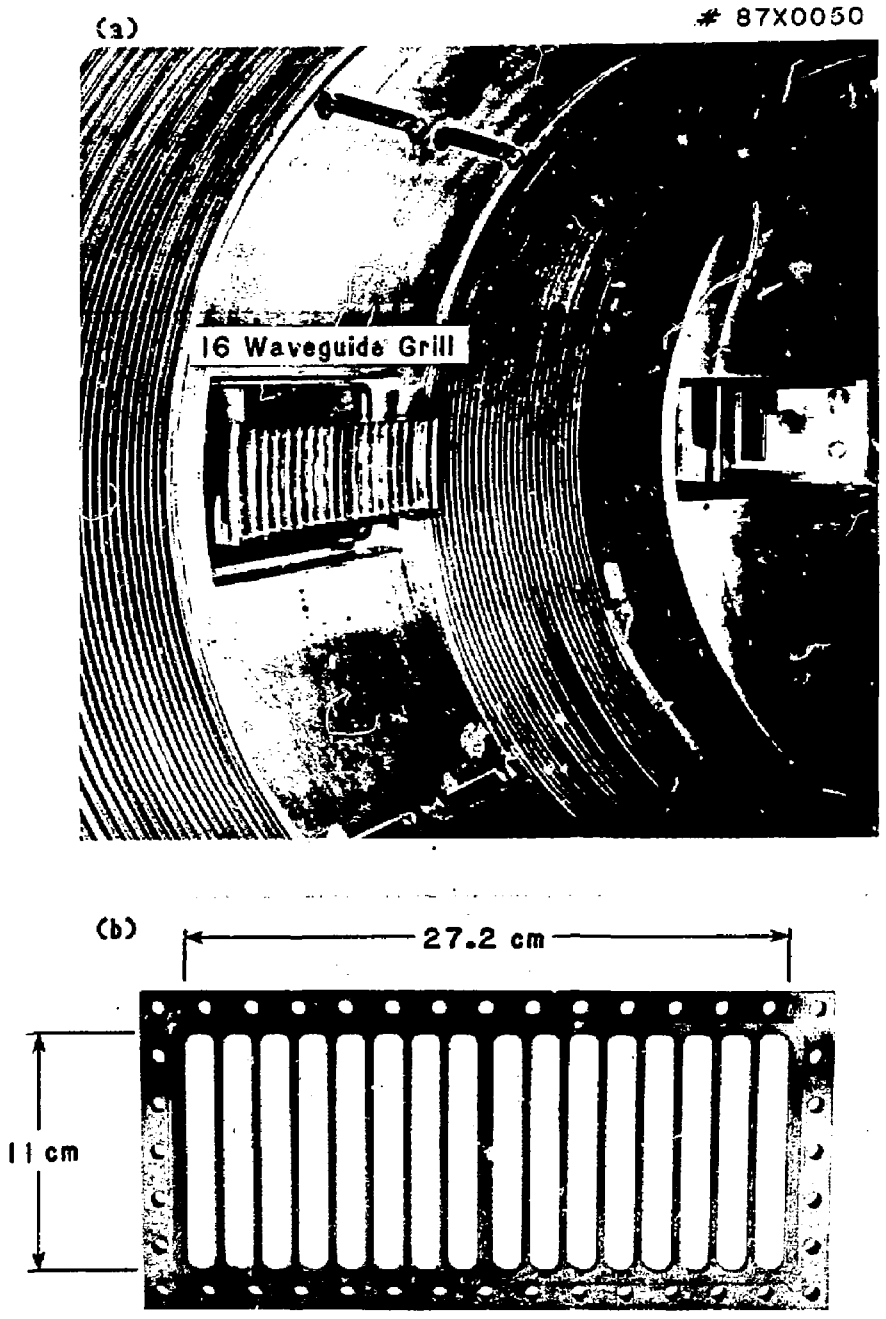

Fig. 1

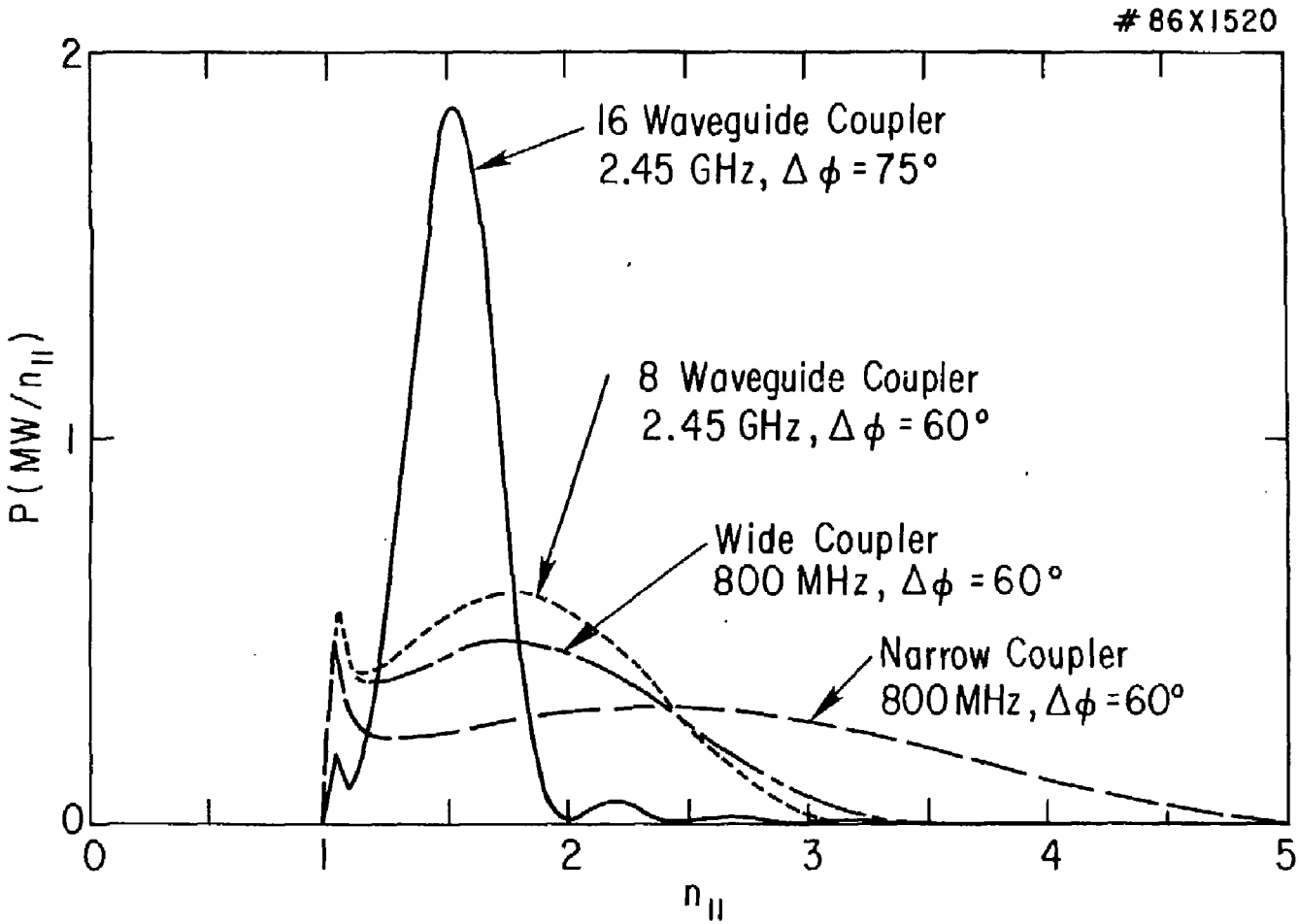
#86X1520
16 Waveguide Coupler
2.45 GHz, Δφ = 75°
8 Waveguide Coupler
2.45 GHz, Δφ = 60°
Wide Coupler
800 MHz, Δφ = 60°
Narrow Coupler
800 MHz, Δφ = 60°
P(MW/n∥)
n∥
0
1
2
3
4
5

Fig. 2

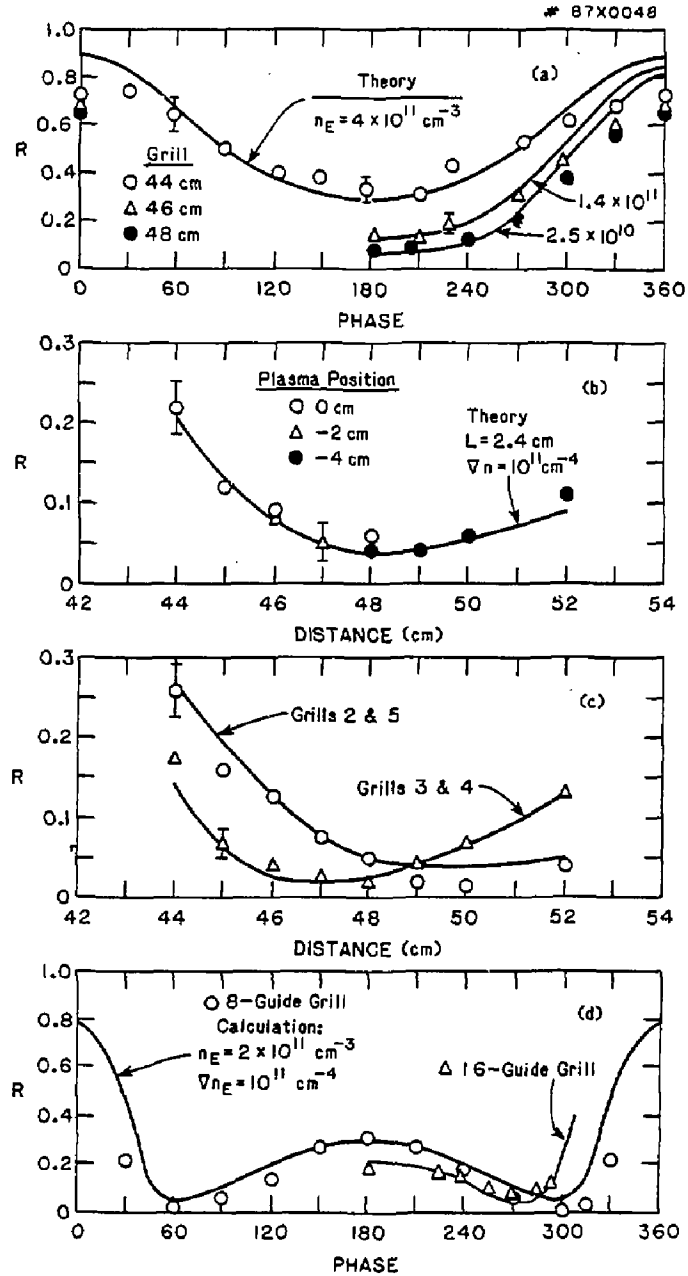
87X0048
(a)
Theory
$n_E = 4 \times 10^{11}$ cm^{-3}
Grill
○ 44 cm
△ 46 cm
● 48 cm
1.4×10^{11}
2.5×10^{10}
R
PHASE
(b)
Plasma Position
○ 0 cm
△ −2 cm
● −4 cm
Theory
L = 2.4 cm
$\nabla n = 10^{11}$ cm^{-4}
DISTANCE (cm)
(c)
Grills 2 & 5
Grills 3 & 4
DISTANCE (cm)
(d)
○ 8-Guide Grill
Calculation:
$n_E = 2 \times 10^{11}$ cm^{-3}
$\nabla n_E = 10^{11}$ cm^{-4}
△ 16-Guide Grill
PHASE

Fig. 3

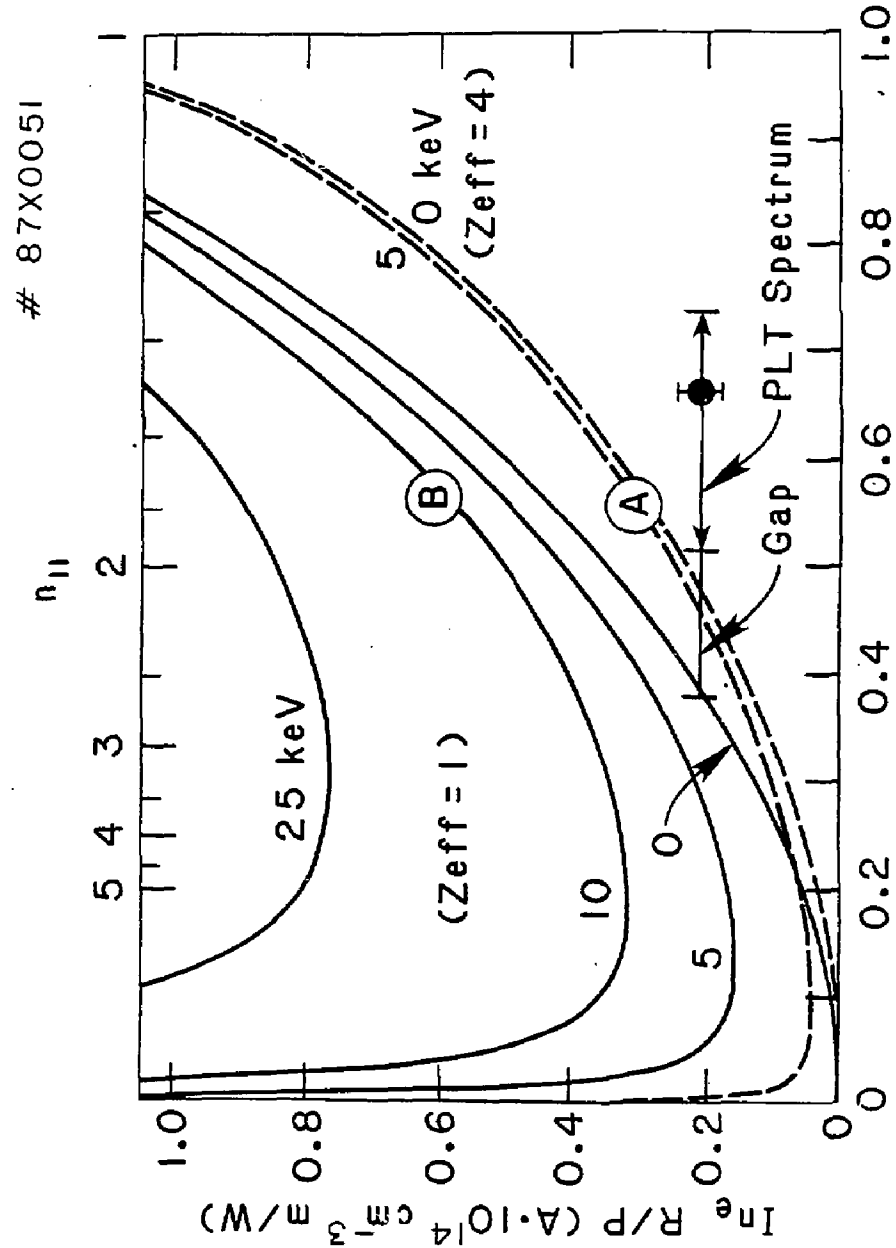
87X0051
$n_{\parallel}$
1
2
3
4
5
25 keV
(Zeff = 1)
10
5
0
B
A
50 keV
(Zeff = 4)
PLT Spectrum
Gap
$v_{\parallel}/C$
0
0.2
0.4
0.6
0.8
1.0
$\ln_e R/P$ ($A \cdot 10^{14}$ cm^{-3} s/W)

Fig. 4

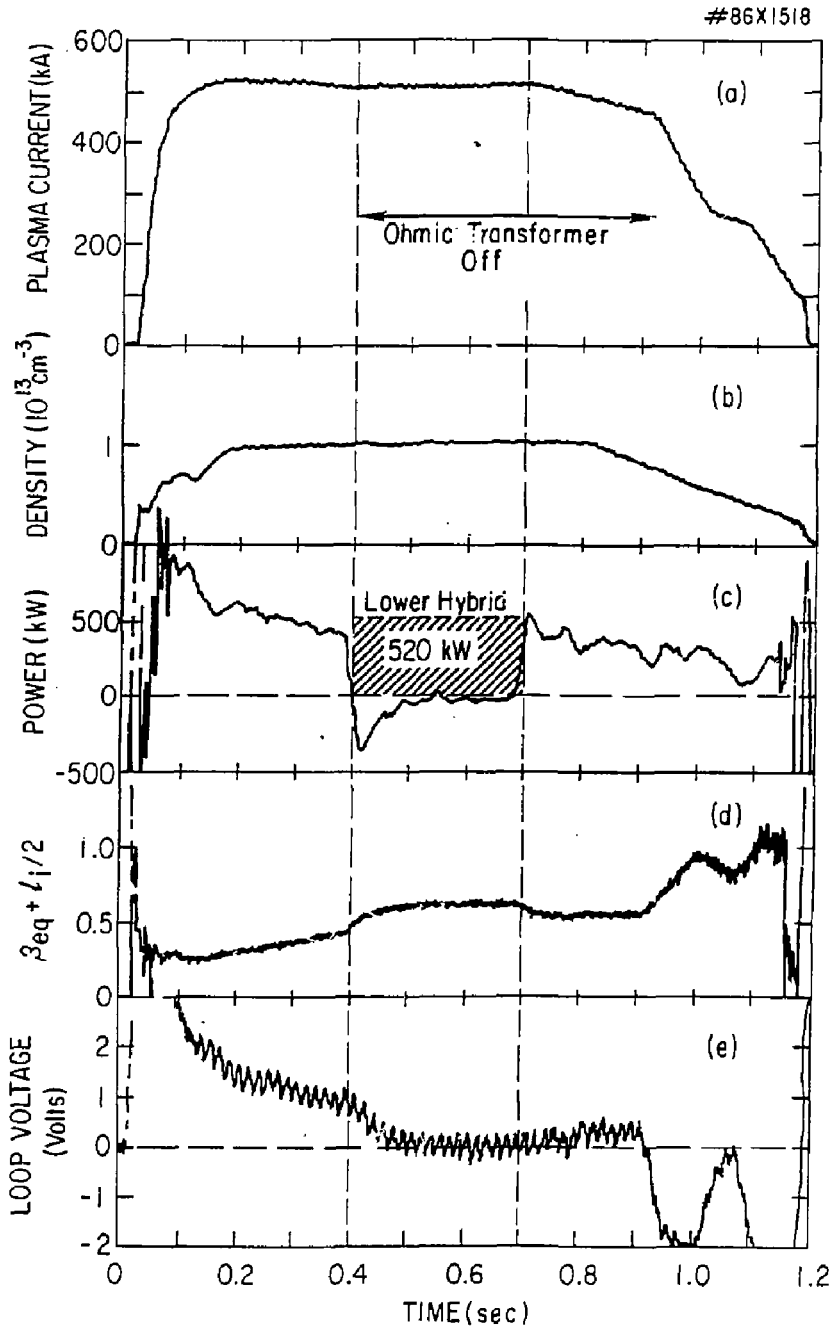
#86X1518
PLASMA CURRENT (kA)
600
400
200
0
(a)
Ohmic Transformer
Off
DENSITY (10^{13} cm^{-3})
1
0
(b)
POWER (kW)
500
0
-500
Lower Hybrid
520 kW
(c)
$\beta_{eq} + l_i/2$
1.0
0.5
0
(d)
LOOP VOLTAGE (Volts)
2
1
0
-1
-2
(e)
0
0.2
0.4
0.6
0.8
1.0
1.2
TIME (sec)

Fig. 5

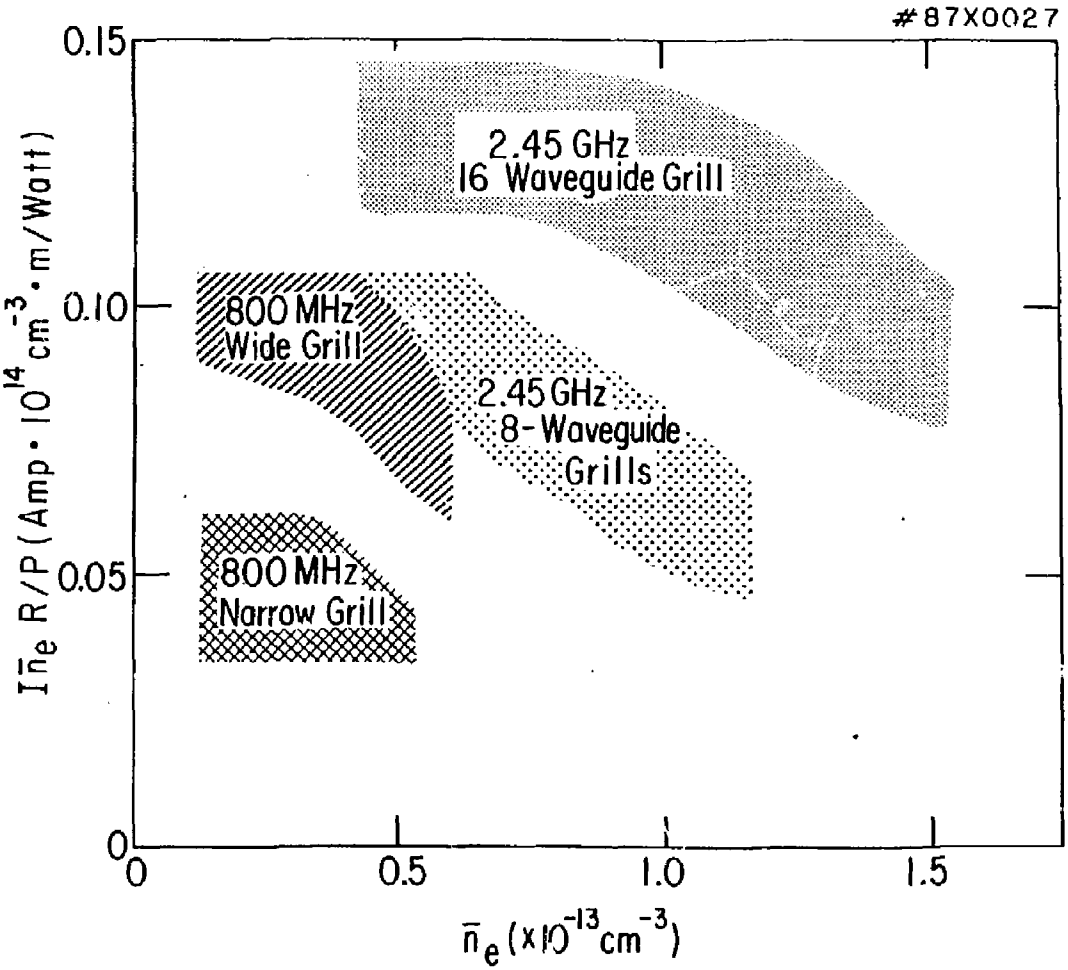
#87X0027
0.15
0.10
0.05
0
0
0.5
1.0
1.5
2.45 GHz
16 Waveguide Grill
800 MHz
Wide Grill
2.45 GHz
8-Waveguide
Grills
800 MHz
Narrow Grill
$I\bar{n}_e R/P$ (Amp • 10^{14} cm^{-3} • m/Watt)
$\bar{n}_e$ (x 10^{-13} cm^{-3})

Fig. 6

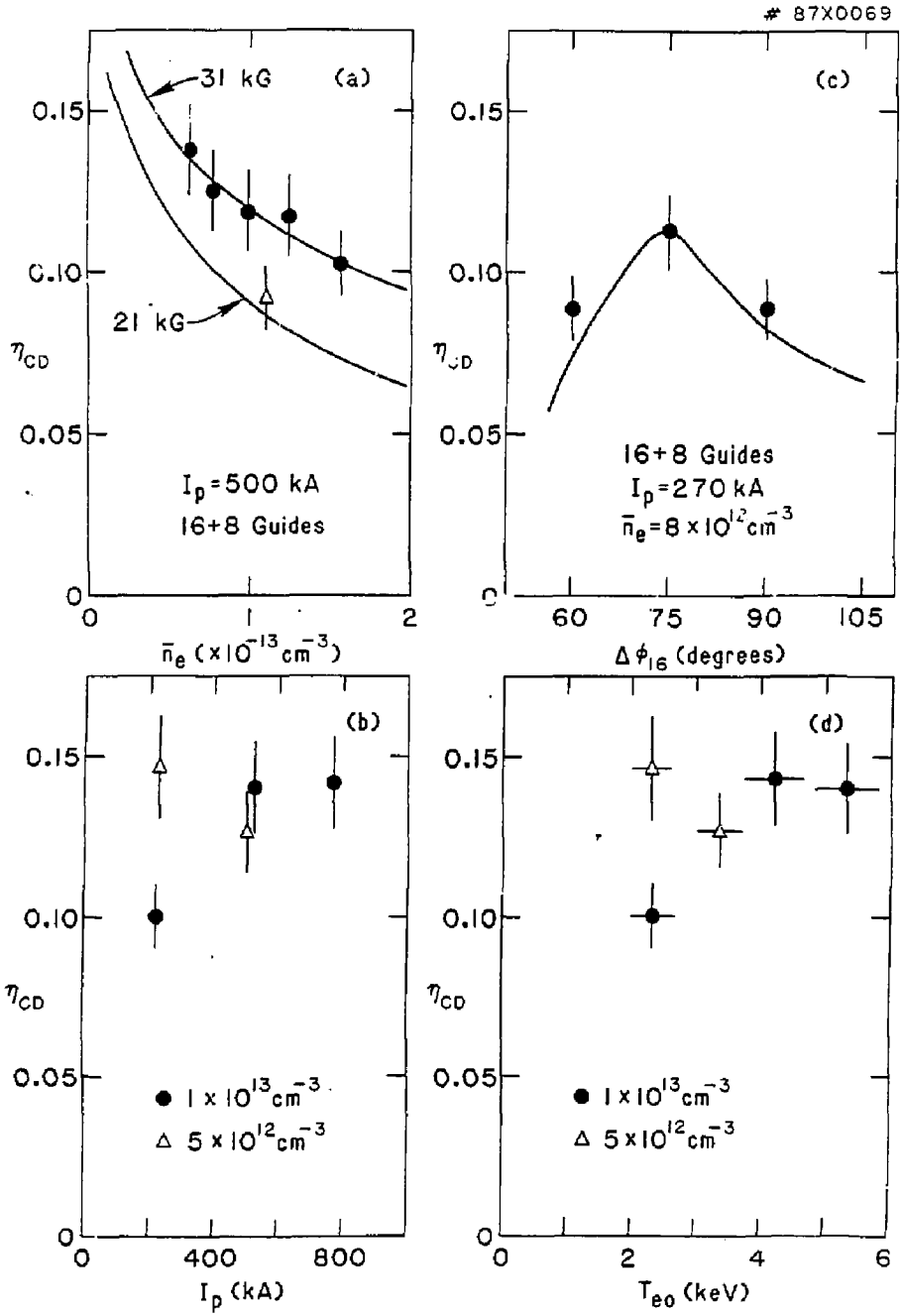
87X0069
(a)
31 kG
21 kG
I_p=500 kA
16+8 Guides
η_{CD}
$\bar{n}_e$ ($\times 10^{-13}$ cm^{-3})
(c)
16+8 Guides
I_p=270 kA
$\bar{n}_e$=8 $\times 10^{12}$ cm^{-3}
$\Delta\phi_{16}$ (degrees)
(b)
● 1 $\times 10^{13}$ cm^{-3}
△ 5 $\times 10^{12}$ cm^{-3}
I_p (kA)
(d)
● 1 $\times 10^{13}$ cm^{-3}
△ 5 $\times 10^{12}$ cm^{-3}
T_{eo} (keV)

Fig. 7

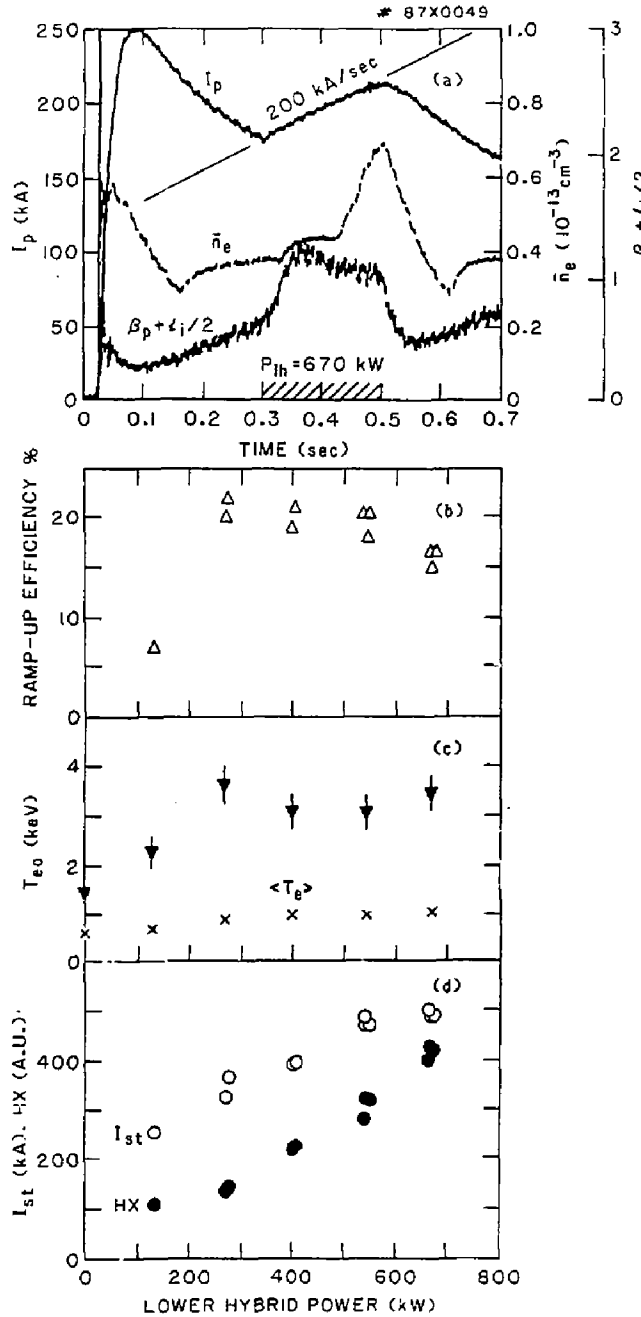
87X0049
I_p
200 kA/sec
(a)
$\bar{n}_e$
$\beta_p+\ell_i/2$
P_{lh}=670 kW
I_p (kA)
$\bar{n}_e$ (10^{-13}cm^{-3})
$\beta_p+\ell_i/2$
TIME (sec)
RAMP-UP EFFICIENCY %
(b)
T_{eo} (keV)
<T_e>
(c)
(d)
I_{st}
HX
I_{st} (kA), HX (A.U.)
LOWER HYBRID POWER (kW)

Fig. 8

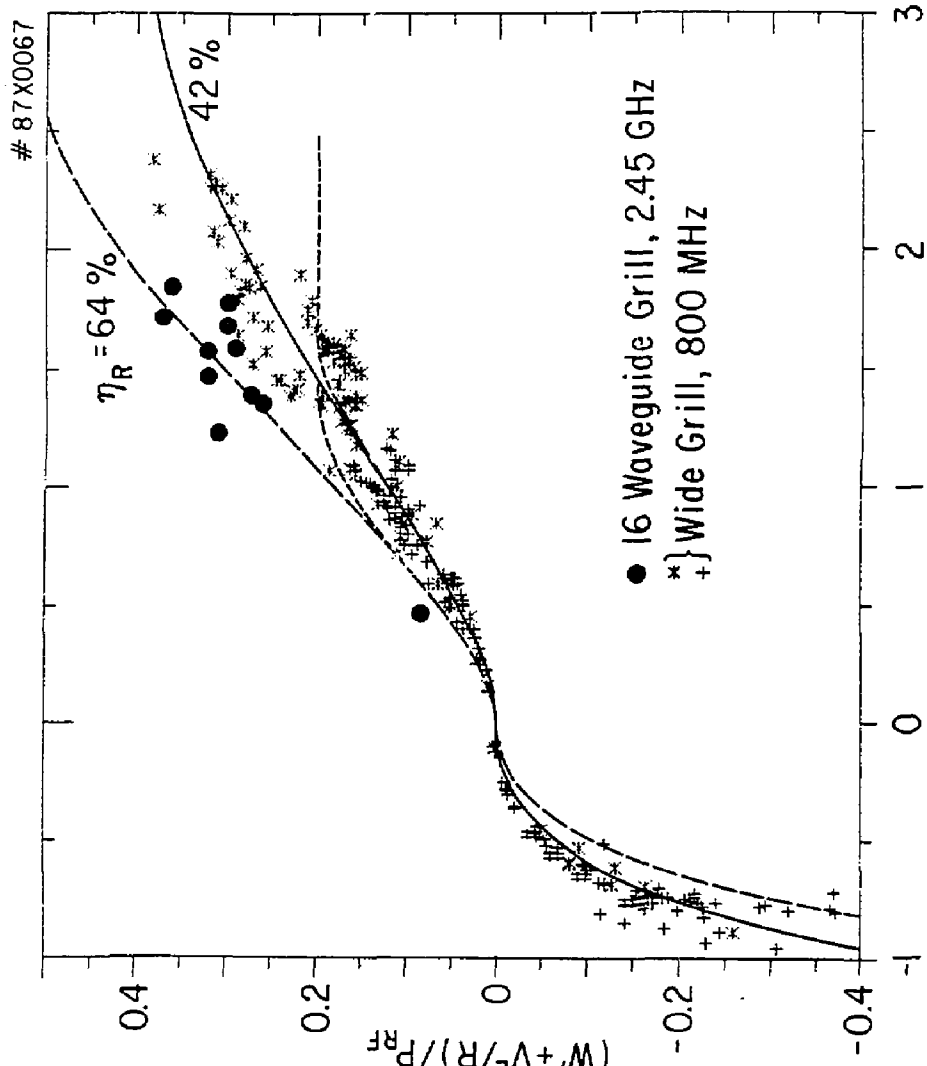
#87X0067
η_R=64 %
42 %
● 16 Waveguide Grill, 2.45 GHz
*} Wide Grill, 800 MHz
+
$(\dot{W}'+V^2/R)/P_{RF}$
v_{ph}/v_R
0.4
0.2
0
-0.2
-0.4
-1
0
1
2
3

Fig. 9

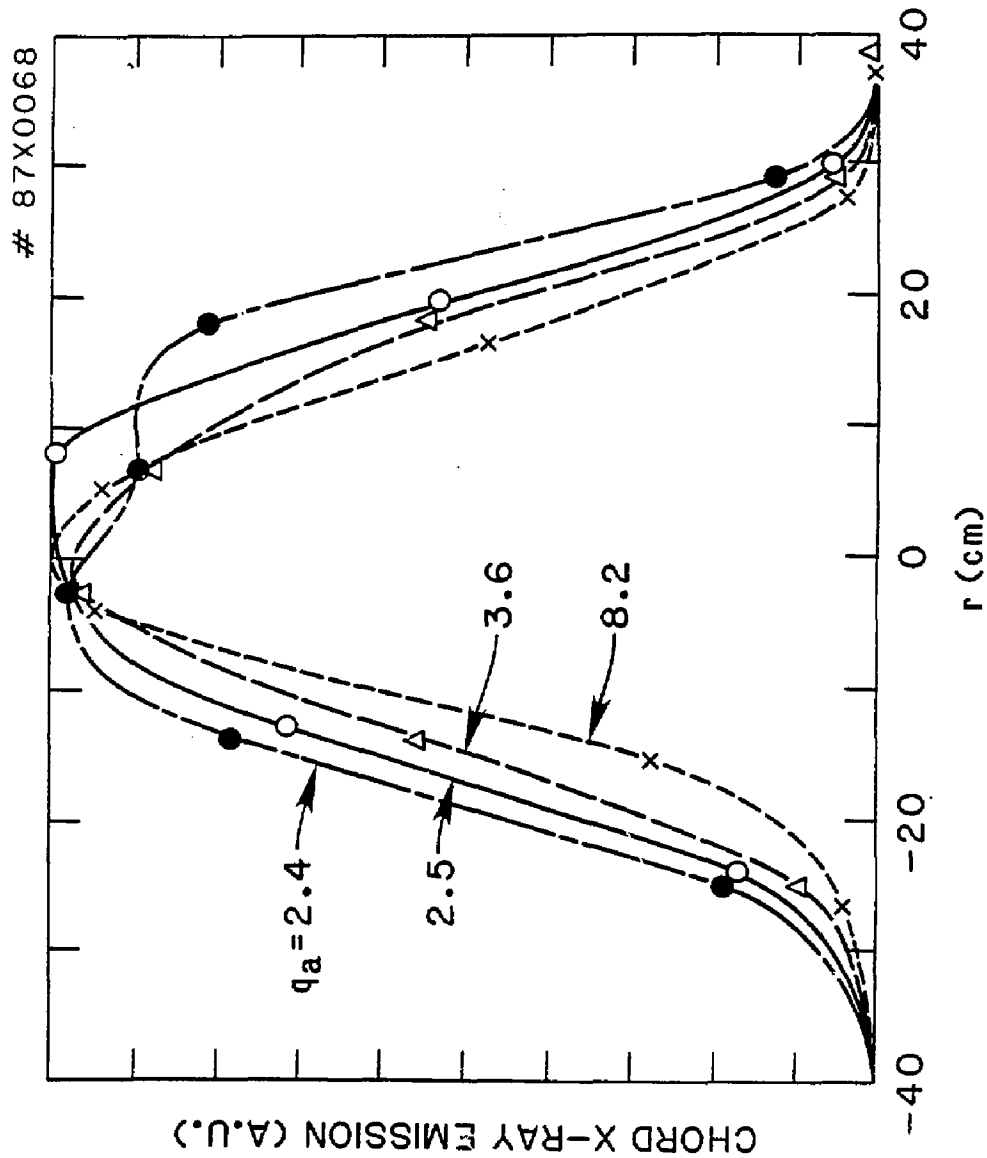

Fig. 10

EXTERNAL DISTRIBUTION IN ADDITION TO UC-20

Dr. Frank J. Paoloni, Univ of Wollongong, AUSTRALIA
Prof. M.H. Brennan, Univ Sydney, AUSTRALIA
Plasma Research Lab., Australian Nat. Univ., AUSTRALIA
Prof. I.R. Jones, Flinders Univ., AUSTRALIA
Prof. F. Cap, Inst Theo Phys, AUSTRIA
Prof. M. Heindler, Institut fur Theoretische Physik, AUSTRIA
M. Goossens, Astronomisch Instituut, BELGIUM
Ecole Royale Militaire, Lab de Phys Plasmas, BELGIUM
Com. of European, Dg XII Fusion Prog, BELGIUM
Prof. R. Boucique, Laboratorium voor Natuurkunde, BELGIUM
Dr. P.H. Sakanaka, Univ Estadual, BRAZIL
Instituto De Pesquisas Espaciais-INPE, BRAZIL
Library, Atomic Energy of Canada Limited, CANADA
Dr. M.P. Bachynski, MPB Technologies, Inc., CANADA
Dr. H.M. Skarsgard, Univ of Saskatchewan, CANADA
Dr. H. Barnard, University of British Columbia, CANADA
Prof. J. Teichmann, Univ. of Montreal, CANADA
Prof. S.R. Sreenivasan, University of Calgary, CANADA
Prof. Tudor W. Johnston, INRS-Energie, CANADA
Dr. C.R. James, Univ. of Alberta, CANADA
Dr. Peter Lukac, Komenskeho Univ, CZECHOSLOVAKIA
The Librarian, Culham Laboratory, ENGLAND
Mrs. S.A. Hutchinson, JET Library, ENGLAND
C. Mouttet, Lab. de Physique des Milieux Ionises, FRANCE
J. Radet, CEN/CADARACHE - Bat 506, FRANCE
Dr. Tom Mual, Academy Bibliographic, HONG KONG
Preprint Library, Cent Res Inst Phys, HUNGARY
Dr. B. Dasgupta, Saha Inst, INDIA
Dr. R.K. Chhajlani, Vikram Univ. INDIA
Dr. P. Kaw, Institute for Plasma Research, INDIA
Dr. Phillip Rosenau, Israel Inst Tech, ISRAEL
Prof. S. Cuperman, Tel Aviv University, ISRAEL
Librarian, Int'l Ctr Theo Phys, ITALY
Prof. G. Rostagni, Univ Di Padova, ITALY
Miss Clelia De Palo, Assoc EURATOM-ENEA, ITALY
Biblioteca, del CNR EURATOM, ITALY
Dr. H. Yamato, Toshiba Res & Dev, JAPAN
Prof. T. Kawakami, Atomic Energy Res. Institute, JAPAN
Prof. Kyoji Nishikawa, Univ of Hiroshima, JAPAN
Direc. Dept. Lg. Tokamak Res. JAERI, JAPAN
Prof. Satoshi Itoh, Kyushu University, JAPAN
Research Info Center, Nagoya University, JAPAN
Prof. S. Tanaka, Kyoto University, JAPAN
Library, Kyoto University, JAPAN
Prof. Nobuyuki Inoue, University of Tokyo, JAPAN
S. Mori, JAERI, JAPAN
M.H. Kim, Korea Advanced Energy Research Institute, KOREA
Prof. D.I. Choi, Adv. Inst Sci & Tech, KOREA
Prof. B.S. Liley, University of Waikato, NEW ZEALAND
Institute of Plasma Physics, PEOPLE'S REPUBLIC OF CHINA
Librarian, Institute of Phys., PEOPLE'S REPUBLIC OF CHINA
Library, Tsing Hua University, PEOPLE'S REPUBLIC OF CHINA
Z. Li, Southwest Inst. Physics, PEOPLE'S REPUBLIC OF CHINA
Prof. J.A.C. Cabral, Inst Superior Tecn, PORTUGAL
Dr. Octavian Petrus, AL I CUZA University, ROMANIA
Dr. Johan de Villiers, Plasma Physics, AEC, SO AFRICA
Prof. M.A. Hellberg, University of Natal, SO AFRICA
Fusion Div. Library, JEN, SPAIN
Dr. Lennart Stenflo, University of UMEA, SWEDEN
Library, Royal Inst Tech, SWEDEN
Prof. Hans Wilhelmson, Chalmers Univ Tech, SWEDEN
Centre Phys des Plasmas, Ecole Polytech Fed, SWITZERLAND
Bibliotheek, Fom-Inst Voor Plasma-Fysica, THE NETHERLANDS
Dr. D.D. Ryutov, Siberian Acad Sci, USSR
Dr. G.A. Eliseev, Kurchatov Institute, USSR
Dr. V.A. Gilkhikh, Inst Electro-Physical, USSR
Dr. V.T. Tolok, Inst. Phys. Tech. USSR
Dr. L.M. Kovrizhnykh, Institute Gen. Physics, USSR
Prof. T.J.M. Boyd, Univ College N Wales, WALES
Nuclear Res. Establishment, Julich Ltd., W. GERMANY
Bibliothek, Inst. Fur Plasmaforschung, W. GERMANY
Dr. K. Schindler, Ruhr Universitat, W. GERMANY
ASDEX Reading Rm, IPP/Max-Planck-Institut fur Plasmaphysik, W. GERMANY
Librarian, Max-Planck Institut, W. GERMANY
Prof. R.K. Janev, Inst Phys, YUGOSLAVIA